


Experimental and Simulated Performance Analysis of Parabolic Trough Collector

A thesis Presented to
SCHOOL OF MECHANICAL AND MANUFACTURING ENGINEERING
Department of Mechanical Engineering
NUST
ISLAMABAD, PAKISTAN



In Partial Fulfillment
Of the Requirements for the Degree
MS Mechanical Engineering

By
Naveed Ahmed
December 2014

Keywords: Heat Transfer Analysis, Parabolic Trough Collector, Solar Thermal Energy, Numerical Modeling, Absorber Tube, Thermal Losses

COMMITTEE MEMBERS

Committee Chair: Dr. Shahid Ikramullah Butt (Supervisor)
SMME, NUST

Dated:

Committee Chair: Asst. Prof Ahmed Sohail (Co-Supervisor)
CEME, NUST

Dated:

Committee Chair: Dr. Mohsin Jamil
SMME, NUST

Dated:

Committee Chair: Dr. Riaz Mufti
SMME, NUST

Dated:

Committee Chair: Dr. Amir Mubashir
SMME, NUST

Head of the Department

Dr. Shahid Ikramullah

Mechanical

Dated:

Principal

Dr. Abdul Ghafoor

School of Mechanical and Manufacturing Engineering

Dated:

ABSTRACT

In this report comparative simulated and experimental heat transfer analysis (HTA) of Parabolic Trough Concentrator (PTC) has been presented by varying operational parameters and using three different configurations of receiver tube. The considered three configurations are i. evacuated absorber tube, ii. Lost vacuum receiver tube with air in the annulus, iii. Bare absorber with broken envelope. Water is used as heat transfer fluid (HTF). The report describes in detail combined conduction, convection and radiation mode of heat transfers in heat collecting element (HCE) for the considered three cases. Computational model has been implemented in MATLAB software and then numerical analysis technique is applied for HTA of receiver tubes. Performance parameters of PTC (heat loss, heat gain, outlet temperature and efficiency) are assessed by evaluating optical model and energy balance model for each absorber case considering meteorological conditions of Islamabad. For fixed geometrical considerations, effect of varying operating parameters ($T_1, \dot{M}, W_v, T_{amb}, A_{apert}, D_1$) and boundary conditions on comparative performance of PTC has been studied. Based on simulation results mini PTC is fabricated and then results are verified experimentally. Manual tracking system was designed to track sun with maximum precision. Under same meteorological conditions performance of PTC is superior by using perfect vacuum tube than other two receiver configurations.

PREFACE

This study is original, unpublished and independent work by the student, Naveed Ahmed.

DEDICATION

All of my thesis work and research is dedicated to my parents. I could not have done this without you and none of my success would be possible without your prayers.

ACKNOWLEDGMENTS

First of all I am thankful to ALLAH Almighty, who gave me knowledge and dedication to work hard for the completion of this thesis. I am grateful to my parents, with their prayers I was able achieve this milestone. I am also thankful to supervisor (Dr. Shahid Ikramullah Butt) and co-supervisor (Asst.Prof Ahmad Sohail), who have been a constant source of support and motivation. Especially I would like to thank my friends who stood by my side with dedication and love. I am also thankful to staff of MRC at SMME for their sincere support during fabrication and experimentation of PTC system.

ORIGINALITY REPORT

COPY RIGHT STATEMENT

- Copyright in test of this thesis rests with the student author. Copies (by any process) either in full, or of extracts, may be only in accordance with the instructions given by author and lodged in the Library of SMME, NUST. Details may be obtained by the librarian. This page must be part of any such copies made. Further copies (by any process) of copies made in accordance with such instructions may not be made without the permission (in writing) of the author.
- The ownership of any intellectual property rights which may be described in this thesis is vested in SMME, NUST, subject to any prior agreement to the contrary, and may not be made available for use of third parties without the written permission of SMME, NUST which will describe the terms and conditions of any such agreement.
- Further information on the conditions under which disclosure and exploitation may take place is available from the library of SMME, NUST Islamabad

TABLE OF CONTENTS

ABSTRACT	ii
PREFACE	iii
DEDICATION	iv
ACKNOWLEDGMENTS	v
Originality Report	vi
COPY RIGHT STATEMENT	vii
LIST OF TABLES.....	xi
LIST OF FIGURES.....	xii
ABBREVIATIONS	xiv
NOMENCLATURE	xv
<u>Chapter 1: INTRODUCTION</u>	18
1.1 Background	18
1.2 Global energy Demand	19
1.3 Energy Demands in Pakistan.....	19
1.4 Thesis Objectives.....	21
1.4.1 Reason/Justification for the selection of the topic	21
1.4.2 Relevance to National Needs.....	22
1.4.3 Advantages	22
1.4.4 Areas of Application.....	23
<u>Chapter 2: Literature Review</u>	24
2.1 Types of CSP technology.....	24
2.2 Existing solar thermal power plants.....	25
2.3 Literature Review	26
<u>Chapter 3: GeometrlC Design of PTC</u>	29
3.1 Working of PTC	29
3.2 Main components of PTC	30
3.3 Geometry Design of Parabolic Trough Collector	31
3.3.1 Concentration ratio	34
3.3.2 Tracing Ideal Focal Length:	34

<u>Chapter 4: Implementation of Numerical Model</u>	37
4.1 Numerical Modeling for Heat Transfer Analysis (HTA) of PTC.....	37
4.2 Evaluation of Hourly Irradiation	40
4.3 Optical Model of PTC.....	42
4.3.1 Solar Energy Absorbed by Receiver Glass Envelope	44
4.3.2 Solar irradiance absorption in absorber tube	45
4.4 Energy Balance Model of Absorber Tube.....	45
4.4.1 Heat Energy Transfer from Absorber Surface to.....	49
4.4.1.1 Flow cases for HTF within absorber tube	49
4.4.1.2 Turbulent & Translational Flow Conditions	49
4.4.1.3Laminar Flow	50
4.4.2 Heat Energy Transfer across Absorber by Conductio.....	50
4.4.3 Heat Energy Transfer from Absorber Surface to Glass Cover	51
4.4.3.1 Heat Transfer by Convection.....	51
4.4.3.2 For Perfect Vacuum Absorber Tube	51
4.4.3.3 For Lost Vacuum Absorber Tube	52
4.4.3.4 Heat Energy Transfer by Radiation	53
4.4.4 Heat Energy Transfer through Glass Envelope by Conduction.....	53
4.4.5 Heat transmission from Envelope Surface to Atmosphere.....	53
4.4.5.1 Heat Energy Transfer by Convection.....	53
4.4.5.2 Heat Energy Transfer by Radiation	55
4.4.6 Heat Energy Transmission for Broken Glass tube.....	55
4.5 Implementation of Numerical Modeling in MATLAB.....	55
4.6 Boundary Conditions	57
<u>Chapter 5: Fabrication for Experimentation Setup of PTC</u>	59
5.1 Fabrication Process	59
5.2 Parabola Reflecting Sheet	59
5.3 Side Rails	60
5.4 Parabolic Ribs	60
5.5 Support Brackets for Receiver Tube.....	62
5.6 Fabrication of Manual Tracking System for PTC	63
5.6.1 Power Screw.....	64

5.6.2 Drive arm	65
5.6.3 Control rod	65
5.6.4 Bracket Bearings:	65
5.6.5 Axle nut.....	66
5.6.6 Wooden Base.....	67
5.7 Hydraulic Scheme.....	67
5.8 Experimentation and Instrumentation.....	69
5.8.1 Thermocouple.....	69
5.8.2 Laser thermal gun	70
5.8.3 Pyranometer	71
<u>Chapter 6: RESULTS & Discussions</u>.....	73
6.1 Simulation Results of Numerical Model.....	73
6.1.1 Trend of output results with variation in Inlet Temperature	74
6.1.2 Trend of output results with variation of Mass flow Rate	76
6.1.3 Trend of output results with variation of Absorber Diameter	77
6.1.4 Trend of output results with variation of Wind speed.....	79
6.1.6 Trend of output results with variation of Aperture Area.....	80
6.2 Comparative experimental & simulated Results	82
6.2.2 Comparative trend of output results with variation in m.....	83
<u>Chapter 7: COncclusion and Recommendations</u>.....	85
7.1 Conclusion	85
7.2 Recommendations	87
Refrences	88
APPENDIX I	92

LIST OF TABLES

Table 1 Commercial Scale isolated CSP thermal power plants.....	25
Table 2 Recommended value of n by month.....	41
Table 3 Error terms considered in optical modeling.....	42
Table 4 Corresponding values of C & m to Reynolds no.....	54
Table 5 Specifications of PTC.....	58
Table 6 Efficiency Drop and Achieved Efficiency of PTC	86

LIST OF FIGURES

Fig.1 World Solar Map.....	22
Fig.2 Basic Working Principle of PTC.....	30
Fig.3 Steam generation via heat exchangers using PTC.....	31
Fig.4 Main components of PTC based thermal power plan.....	32
Fig.5 Convergence at focal point.....	33
Fig.6 Geometry parameters of PTC.....	33
Fig.7: Relationship between focal length and rim angle.....	34
Fig. 8.a perfect alignment case.....	36
Fig.8.b in case of misalignment.....	36
Fig.9 (a) For Broken (b) For Lost Vacuum (c) For.....	39
Fig.10 General Algorithm flow chart scheme	40
Fig.11 1-D steady state energy balance model.....	48
Fig.12 Equivalent thermal resistance model.....	48
Fig.13 Reflecting sheet with parabola ribs for PTC.....	60
Fig.14 Fixing of side rails with wooden ribs along parabola sheet.....	61
Fig.15 Dimensions of Parabola ribs.....	62
Fig.16 (a) Ready parabolic Rib (b) CNC machine used for parabola ribs.....	62
Fig.17 Precise fabrication of wooden ribs for PTC.....	63
Fig.18 Fixing of bearings in wood.....	64
Fig.19 Manual Tracking Drive Assembly.....	65
Fig.20 Drive Arm with Axle nut.....	66
Fig.21 Bracket Bearing.....	67
Fig.23 (a) Wooden Base (b) Tracking Assembly.....	68
Fig.24 Hydraulic Scheme.....	69

Fig.25 Hydraulic Scheme Used for PTC Experimentation.....	70
Fig.26.Placement of thermocouple.....	71
Fig.27 Absorber surface temperature measurement using thermal laser gun.....	72
Fig.28 Solar Irradiance measurement using Pyranometer.....	72
Fig. 29 Experimental Setup of PTC along with Manual Tracing System.....	73
Fig.30. Affect fluid inlet temperature on the performance of PTC.....	75
Fig.31 (a) Comparative Percentage drop in efficiency.Fig.31 (b) comparative	76
Fig.32. Affect of Mass flow rate on the performance of PTC.....	77
Fig.33 (a) Comparative Percentage drop in efficiency.Fig.33 (b) comparative	78
Fig.34. Affect of Absorber diameter on the performance of PTC.....	79
Fig.35 (a) Comparative Percentage drop in efficiency.Fig.33 (b) comparative	79
Fig.36. Affect of wind speed on the comparative performance of PTC.....	80
Fig.37 (a) Comparative Percentage drop in efficiency (b) comparative Maximum	81
Fig.38. Affect of Aperture area on the performance of PTC.....	82
Fig.39 (a) Comparative Percentage drop in efficiency (b) comparative	83
Fig.40 comparative experimental and simulated performance of PTC	84
Fig.41 comparative experimental and simulated	85

ABBREVIATIONS

HCE Heat Collector Element

PTC Parabolic Trough Collector

CSP Concentrated Solar Power

HTF Heat Transfer Fluid

IEA International Energy Agency

MTOE Million Tons of Oil Equivalents

KWH Kilo Watt Hour

MW Mega Watts

CDM Clean Development Mechanism

DSG Direct Steam Generation

HTA Heat Transfer Analysis

MRC Manufacturing Resource Centre

CNC Computer Numerical Controlled

DMM Digital Multi meter

NOMENCLATURE

Nomenclature	
L_{apert} Aperture length (m)	$\dot{Q}_{3solabs}$ incident solar energy on absorber surface (W/m)
A_{apert} Aperture Area (m ²)	\dot{Q}_{36conv} Convection losses from receiver surface to ambient atmosphere (W/m)
\dot{m} Mass flow rate (Kg/sec)	\dot{Q}_{37rad} Irradiative losses from receiver surface to ambient atmosphere (W/m)
I_b Beam solar irradiance (W/m ²)	$\dot{Q}_{Heatgain}$ Heat gain of PTC (W/m)
\dot{Q}_{12conv} convection heat transfer from absorber inner surface to HTF (W/m)	$\dot{Q}_{Heatloss}$ Heat losses (W/m)
\dot{Q}_{23cond} conduction heat transfer in absorber (W/m)	D_1 absorber inside diameter (m)
$\dot{Q}_{5solabs}$ Incident Solar Irradiation absorption by outer glass envelope (W/m)	D_2 absorber outside diameter (m)
\dot{Q}_{si} Incident solar irradiation on receiver (W/m)	D_3 inner glass envelope diameter (m)
$\dot{Q}_{3solabs}$ incident solar irradiation on absorber outer surface (W/m)	D_4 Outer glass envelope diameter (m)
\dot{Q}_{56conv} convection thermal loss from outer glass envelope to ambient air	h_1 convection heat transfer coefficient of HTF at the temperature of T1 (W/m ² -K)
\dot{Q}_{57rad} Radiation thermal loss from outer glass envelope to sky	h_{34} heat transfer coefficient by convection at T ₃₄ (W/m ² -K)
\dot{Q}_{34conv} convection heat transfer b/w absorber and	Nu_{D_1} Nusselt number based on D_1
	Nu_{D_4} Nusselt number based on D_4
	T_{out} Temperature of outer surface (K)

glass envelope (W/m)	T_{Inn} Temperature of inner surface (K)
\dot{Q}_{34rad} Radiation heat transfer b/w envelope and absorber surfaces (W/m)	T_1 Inlet HTF temperature (K)
\dot{Q}_{45cond} conduction in glass envelope	T_2 Receiver inside surface temperature (K)
P_a Annulus pressure (mmHg)	T_3 Receiver outside surface temperature (K)
ν Kinematic viscosity (m ² /sec)	T_{34} average temperature $(T_3 + T_4)/2$ (K)
h_{56} convection thermal coefficient for air at T_{56} (W/m ² -K)	T_{56} $(T_5 + T_6)/2$ (K)
g Constant for gravity (9.81) (m/s ²)	T_4 Envelope surface inside temperature (K)
b interaction coefficient	T_5 Envelope Surface outside temperature (K)
a accommodation coefficient	T_6 Ambient Temperature (K)
Re_{D_1} Reynolds number based on D_1	T_7 effective sky temperature (K)
Ra_{D_2} Rayleigh number at D_2	K_1 Thermal conductivity of the HTF at T_1 (W/m-K)
K_{std} Thermal conductivity of gas at STP (W/m-K)	K_{34} Thermal conductivity of vacuum gas at T_{34} (W/m-K)
D_{Inn} Inner diameter (m)	K_{45} Thermal conductivity of vacuum gas at T_{45} (W/m-K)
K_{56} Thermal conductivity of air at $(T_5 - T_6)/2$ (W/m-K)	D_{Out} Outer diameter (m)
f friction factor for absorber surface	α_{env} Absorptance of the glass envelope
\dot{Q}_{cond} conduction heat transfer (w/m)	α_{abs} Absorptance of absorber
K_{cond} Thermal conductance (W/m-K)	$\eta_{optical}$ Optical efficiency of PTC (%)
Greek Letters:	η_{PTC} Efficiency of PTC (%)
	β volumetric gas expansion coefficient (1/K)
	τ_{env} transmittance of the outer glass cover

ε_3 emissivity of receiver selective coating ε_4 emissivity of glass envelope α Thermal diffusivity (m^2/sec) γ Ratio of specific heats η_{abs} Absorptance of absorber	λ Mean-free-path for a molecule (cm) σ Stefan-Boltzmann constant ($\text{W}/\text{m}^2\text{-K}^4$) δ Molecular diameter (cm) η_{env} Optical efficiency at glass envelope (%)
--	--

CHAPTER 1

INTRODUCTION

1.1 Background

Energy is considered as soul of this advance machine era. Human race has developed the world to unbelievable heights during current age. Automated machines have made the world easy place to live for humans but it requires non-stop sustainable energy supply to continue technology advancement. Higher rate of development and progress in a country means higher amount of energy utilization. Same is the reason that socioeconomic development of a region or country is depicted by per capita energy utilization [1].

It has become a chestnut situation that the earth is running short of conventional fuels resources and world is looking for alternate energy resources. The sun energy has a massive prospect to address the global energy concerns. Parabolic trough collector (PTC) based thermal power plants is one such subcategory example and can efficiently be used in industrial sector for power generation ranging from 50 to 200 Mega-Watts. Pakistan is situated in the belt where there is an abundant amount of solar insolation is available. The average amount of solar insolation is around 1900- 2000 KWh/m² per annum which makes Pakistan suitable to get benefit from this technology. The huge savings of fuel (Natural Gas or Diesel Oil) can be done and hence huge amount of monetary benefits can be achieved.

In addition to environmental issues, there are a number of other influencing reasons making world to go for alternate energy resources, like unstable oil prices in international market and depleting fossil fuel resources. We need indispensable approach to have sustainable energy source. Green energy solutions like Solar (solar thermal & solar PV), hydropower, wind energy and bio-mass are best alternate available options which are long lasting, easily available and of course environmentally clean solutions.

1.2 Global energy Demand

World Energy Outlook 2009 stated that there oil consumption will increase from twelve thousand million tons to sixteen thousand and eight hundred million tons because of raised energy demand up to 40% during 2007 to 2030 which comes to be 1.5% per annum [2]. Approximately Two third of the total energy requirement is related to thermal energy where as only one third is related to electricity. The major source of this heat energy consumption is in industrial processes and commercial sector.

International Energy Agency (IEA) stats say that the total primary energy consumption of world has risen to 12, 1717 Million Tons of Oil Equivalent (MTOE) during 2010 which was 6,107 MTOE during 1973. This total primary energy supply is met by Oil resources 32.4%, Coal/peat resources 27.3%, Bio-fuel energy 10%, Hydro 2.3%, Nuclear energy 5.7%, Natural gas 21.4% and miscellaneous 0.9% [3]. Earth is running is running short of fossil fuel reservoirs at exponential pace and their cost per Kilo Watt Hour (KWH) is unpredictably impulsive which intern is influencing negatively world economy. The use of these existing conventional fuel resources is causing pollution problem, irrecoverable loss to eco system and unpredictable climatic changes to earth.

The major cause of global warming is the production of carbon dioxide as the result of burning of fossil fuels. During 2008, approximately 81.4% of global energy demand was met by burning fossil fuels (Coal, Oil and gas) which produced around 29.5 thousand million tons of carbon dioxide, a major contribution to global warming [4].

1.3 Energy Demands in Pakistan

Pakistan is under-developed country with a population of about 181.3 million [5] Pakistan is blessed with gigantic natural energy resources but in spite of this fact, the country is suffering severe power crisis. Electricity power short fall during 2010 was observed up to 4522 Mega Watt (MW) and becoming worse with the passage of time. During 2011 Energy deficit up to 7000 MW was observed [6]. Overall energy shortage in Pakistan has adversely affected every aspect of life and around 40,000 villages are deprived of electricity in the country. [7]. Present gas and oil reservoirs of Pakistan are

only 48.8% and 5% of the total energy. To meet primary energy demand of 63.09 MTOE during 2010, the country imported 21.64 MTOE [8]. At present energy utilization rate these resources are likely to be exhausted in sixteen and thirteen years respectively. This will cause huge dependence on imported fossil fuels causing energy security threat to Pakistan. The situation clearly depicts that Pakistan dreadfully needs to go for alternative energy solutions to overcome power crisis on war footing basis.

Pakistan has outstanding potential of sustainable variety of energy resources. Identification and utilization of this potential is very important to make this country energy self-dependent. With the available alternate energy resources in Pakistan, government should make efforts priority wise in following order 1. Solar Energy, 2. Bio-gas resources, 3. Micro hydel, 4. Wind energy and 5. Geo-thermal [9]. As depicted in world solar map issued in Fig.1 [10], Pakistan is located in the 2nd highest solar rich region which receives solar irradiation around 1900-2000KWh per square meter [11]. Lack of solar energy research under local meteorological conditions, infrastructure and absence of solar manufacturing industry are main hurdles in the propagation of subject technology. It has led to higher per unit cost of solar energy and ultimately great hesitation to the adoption of this technology at consumer level.

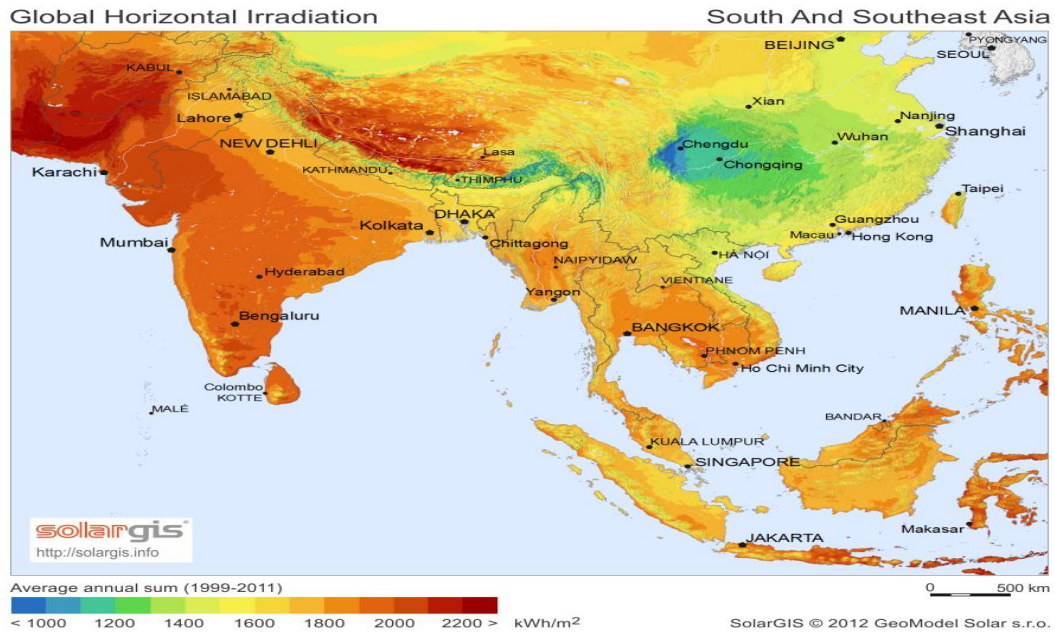


Fig.1. World Solar Map

1.4 Thesis Objectives

- To develop a simulation model for PTC
- Heat transfer analysis of receiver using different configurations of absorber tube.
- Based on optical model and energy model, Comparative performance analysis of miniature version of PTC for three different cases.
- Fabrication of mini PTC based on simulation results of numerical model.
- Experimentation and data extraction by varying boundary conditions.
- Experimental and simulated comparative performance analysis

1.4.1 Reason/Justification for the selection of the topic

Pakistan is facing serious pressing energy crisis and it is prevailing with the passage of time. All major sectors of the country are being affected due to this. In order to overcome current energy crisis, there is a need to go for alternate and green energy resources. Pakistan is a country which receives daily huge amount of solar thermal energy. It can significantly contribute to our national energy needs. To extract this huge potential of

solar energy for a developing country like Pakistan, there is a vast need of research in solar thermal sector. CSP technology is a major part of solar thermal energy. Designing of concentrated collectors according to Pakistani environmental conditions is very important for the success of subject technology. Testing and evaluation of different types of concentrated collectors will give better idea to the designers how to go for more efficient design. This thesis research will definitely contribute its part in reducing energy crisis by presenting study analysis on PTC under metrological conditions of Pakistan.

1.4.2 Relevance to National Needs

Energy sector of Pakistan is considered to be under-developed. Current power crisis is a plague that is poisoning many sectors productivity and growth, increasing circular debt on government. The root problem is energy generation which never took place proportionately with the rising demand. This increased demand of energy can be met if we concentrate on renewable energy resources particularly solar thermal energy along with other conventional sources. Pakistan is situated in the belt where there is abundant amount of solar insolation is available, the average amount of solar insolation is around 1900- 2000 KWh/m² per annum which make Pakistan suitable to get benefit from this technology. The results of subject thesis topic will provide fruitful study analysis for the propagation of solar thermal technology in Pakistan

1.4.3 Advantages

Sun energy is free and you do not have to pay for it. CSP technology is more suited for Pakistan region as it receives huge amount of solar thermal energy daily. Comparative performance study of mini PTC using three configurations of PTC will give better idea to designers to calculate overall thermal losses and ultimately efficiency of solar thermal plant under meteorological conditions of Pakistan. Solar thermal plant performance is significantly affected by each variation in configuration. In case of any mishap during the operation of solar thermal plants, HCE loses vacuum or can be broken. For cost effectiveness, it becomes very important to quantify how much thermal efficiency has been degraded to help owners when the best time to replace is degraded solar collector

receiver for cost effectiveness. Use of PTC based plants can help to replace considerable amount of fossil fuels (Natural Gas/Coal/Fuel Oil) and the environment hazards related with them. More utilizing the CSP technology means less emissions of CO₂ which help them to get benefit from CDM program for larger plants which is incentive based.

1.4.4 Areas of Application

PTC based plants use specially designed mirrors to concentrate the sun's rays to receiver and transfer thermal energy to working fluid to generate steam, which intern can be used for variety of applications.

- Commercial scale PTC plants are used for electricity generation.
- Boilers are extensively used for steam generation to be used in different manufacturing processes. CSP concentrators can be used to generate steam for industrial applications and can replace boilers to meet thermal energy of a factory like leather industry, Textile, Pharmaceutical, chemical industry etc.
- Mini PTCs can be used for domestic water heating and space heating etc
- PTC can exclusively be used for space heating & cooling systems.
- CSP concentrators also find their applications in heat based water desalination processes.
- CSP plants can also be used to produce steam to inject into mature and heavy oil fields for thermal enhanced oil recovery.

CHAPTER 2

LITERATURE REVIEW

2.1 Types of CSP technology

Solar power generation technologies (Solar thermal & Solar PV) are now mature and established alternate energy resources. Large numbers of projects of mega watt power generation are in progress in many countries. Solar power generation is the fastest growing technology of all renewable energy technologies [12]. Among solar thermal practices Concentrated Solar Power (CSP) technology is on a big way of adaption. Capacity of concentrated solar thermal power plants was increased to 35% by the addition of more than 450 MW projects. Mostly projects were parabolic trough collector (PTC) based thermal power plants [13]. Similarly, out of 232 GW world total consumption, 27% was met by solar thermal heating and cooling. Solar thermal technology is more flexible and efficient and can easily be stored and hybridized with other power sources as compared to solar PV [14].

There are different types of CSP collectors being used in thermal power plants [15]

- i) PTC
- ii) Dish Sterling Systems
- iii) Linear Fresnel Reflectors
- iv) Solar Power Towers

Parabolic trough power plants constitute the biggest share of the installed concentrating solar power technology. Distinguishing between parabolic trough power plants, Fresnel power plants, solar tower power plants and dish/Sterling systems, the parabolic trough power plants provide over 90% of the capacity of concentrating solar power plant technology that is in operation or in construction in September 2010.

2.2 Existing solar thermal power plants

Among the planned additional capacity (at the same date) more than 50% are constituted by parabolic trough power plants. The **Table-1** shows the absolute numbers and the shares of the four technology types among the plants in operation, in construction, in the planning stage, and, finally, the sum of all of them. PTC based thermal power plants has majority contribution in the installed CSP technology. PTC plants contribute more than 90% of solar thermal technology which are in operation or under erection in 2010. More than 50% planned CSP projects are PTC thermal plants. [16]

Some of the large scale standalone concentrated solar thermal power plants operating in different parts of the world are listed in **Table-1**

Table-1 Commercial Scale isolated CSP thermal power plants operating

Plant Name	Location	Capacity	Technology
Ivanpah Solar Power Facility	California Mojave Desert	392 MW	PTC
Solana Generating Station	Arizona	280 MW	PTC
Genesis Solar Energy Project,	Colorado Desert, California	250 MW	PTC
Solaben Power Station	Spain	200 MW	PTC
Solnova Solar thermal Power Station,	Spain	200 MW	PTC

Martin Next Generation Solar Energy Centre	Florida, USA	75 MW	Steam input into combined cycle
Puerto Errado	Spain	31.4 MW	Linear Fresnel Reflectors
Maricopa Solar	Arizona, USA	1.5 MW	Dish Sterling Systems
PS-20 Solar Power Tower	Spain	20 MW	Solar Power Tower

2.3 Literature Review

Significant numbers of research studies of solar thermal power plants based on simulation and experiments have been published since 1970. Optimization of performance parameters of PTC under particular climatic and operating conditions has been the focused challenge in these studies [17]. Designers and researchers tried to improve parametric efficiency of PTC under different operating conditions. Some of them focused on innovative designs to optimize cost and performance while others focused on experimental analysis to enhance receiver tube durability, selective coating material using advance instrumentation techniques [15]. Majority of these experimental and simulation performance analysis carried out are one dimensional based on first or second law of thermodynamics [18]

Receiver tube of PTC plays important role in performance optimization and heat loss control. CSP based Solar power plants which operate steam at very high temperature are being used for power generation. However there are low and mid temperature thermal applications which need simple & cost effective designs [19]. Advance research on selective coatings has resulted in high temperature receiver tubes at about 350 °C. These selective coatings are applied to exposed absorber surface and envelope surface to reduce thermal losses [20]. Condition of absorber tubes for a solar thermal power plant can be compromised any time during operation. Schott experimented PTR70 HCE in NREL for three types of receiver tubes i). Broken ii). lost vacuum iii). Hydrogen and showed its effect on the performance of plant [21].

Simulation model of PTC based on 1-D energy balance was verified by comparing its results with experimental results. The performance of thermal plant was evaluated by sensitivity analysis based on heat transfer fluid and corresponding Reynolds number. The effect of shielding on upper portion of annulus b/w absorber surface and envelope is also presented [22]. Thermal and optical performance of commercial scale PTC was calculated by introducing a field test method. Optical efficiency, longitudinal and transverse angle modifiers are used to evaluated optical performance. Comprehensive testing method has been described in the article to measure different performance parameters [23]. Priority score method was employed for material selection to be used in fabrication of PTC system and then Taguchi's L-9 array method was used for experimental analysis. Optimized input parameters are identified by using desirability function and then varying operational parameters [24]. A detailed exergy analysis as a

function of operational conditions and environmental variables was presented to check overall performance of PTC system. Results revealed that majority of thermal energy losses occur at absorber tube and efficiency is highly reduced due to optical factors or errors [25].

In current thesis work comparative simulated and experimental performance of PTC is evaluated by varying different operating conditions for three different configurations of absorber tube. Present study reveals that efficiency of PTC is significantly affected by each variation in configuration of HCE and therefore it becomes important to replace the compromised receiver in field for cost effectiveness. Small scale PTC is used to heat water which can further be utilized for practical applications like domestic hot water consumption, space heating, process heating etc.

GEOMETRIC DESIGN OF PTC

3.1 Working of PTC

PTC technology consists of parabola shaped reflecting mirrors curved around uni-axis. Single axis focal line collects all the reflected solar rays from parabola sheet to parallel absorber tube. Tracking mechanism is integrated with PTC to ensure proper tracking of sun from dawn to dusk for maximum efficiency. Basic configuration idea is shown in **Fig.2**

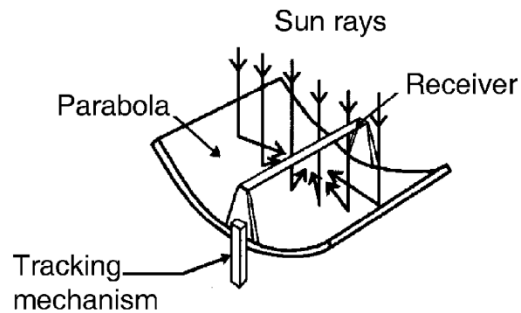


Fig.2 Basic Working Principle of PTC

Thermal energy storages can be integrated with PTC based thermal plants to enhance the operation hours of plant and smoothen output. PTC is the most mature CSP technology among all other. Currently designed PTC power plants use oil as HTF which is then used for water pre-heating or steam generation via installed heat exchangers using combined power cycle or Rankin cycles as shown in **Fig.3**. New area of research for engineers is direct steam generation (DSG). In DSG, water is used as working fluid which is directly heated in absorber tube to produce steam without involving any heat exchanger. DSG is a cheaper solution for power generation using CSP technology as complexity and some components of the system are eliminated. Lower thermal losses and lower average temperatures are some influencing factors to improve the performance of DSG solar

field. However these thermal power plants need to integrate with storage systems for sensible and latent energy storage

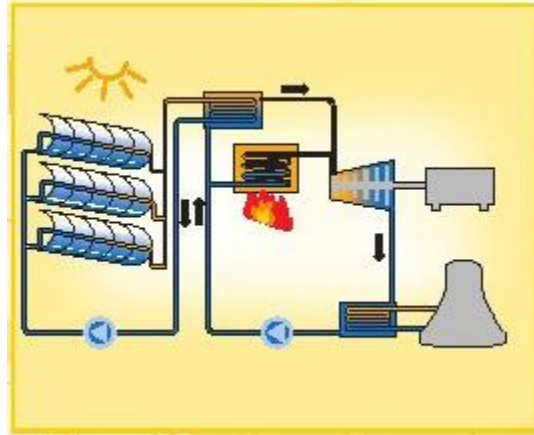


Fig.3 Steam generation via heat exchangers using PTC. Courtesy [16]

3.2 Main components of PTC

The main components and structure of energy flow in PTC based thermal power plant is illustrated in **Fig.4**. Direct solar irradiation is focused on absorber which converts it into thermal energy. Thermal power is converted to steam vapour pressure, which then induces Kinetic energy. This kinetic energy results to produce final product of thermal power plant that is electrical power. Different components of thermal plant bring about these energy changes. HTF and thermal storages are the carrier of thermal energy. Steam generators produce vapor pressure energy. Phase conversion between gas and liquid takes place in cooling system. Rotational energy is converted to electrical energy by electric generator.

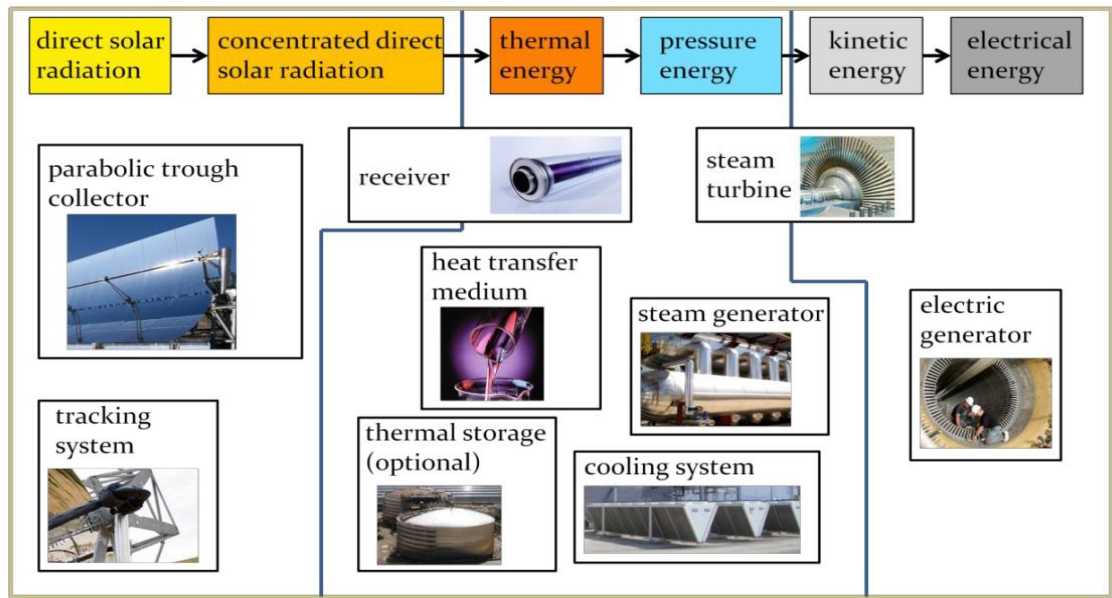


Fig.4 Main components of PTC based thermal power plant .courtesy [16]

3.3 Geometry Design of Parabolic Trough Collector

Focal line is backbone of parabolic trough collectors which comprises of continuous focus points of PTC cross sections. Parabolic sections have the property that radiation entering the parabola plane is reflected back at single line called focal line. This idea can be used to device a PTC capable of suggesting a focal line out of infinity parabolic geometry sections.

Distance of convergence point of incident rays to vertex of PTC is called focal length as shown in **fig.5** and normally designated by ' f '. Analytical representation of parabolic shape is

$$y = \frac{1}{4*f} * x^2 \quad \text{-----}(1)$$

Where x represents aperture width and y represents distance of focal length from vertex of PTC.

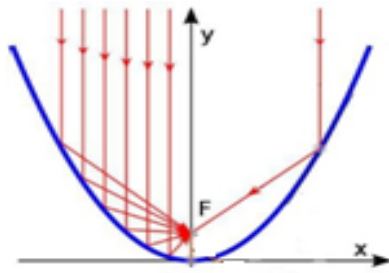


Fig.5 Convergence at focal point

Equation-1 shows that for a fixed length and width, the only factor on which parabola depends is focus point or focal line. When this equation is implemented to make PTC, the considered parameters expand to four which are used to characterize the shape and size of PTC as shown in **Fig.6**. These are briefly describe below

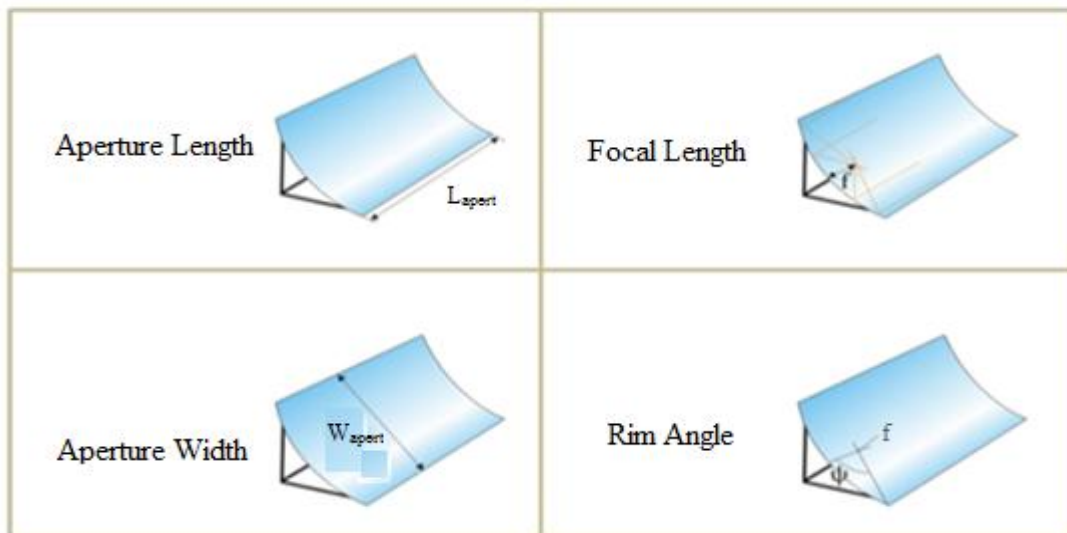


Fig.6 Geometry parameters of PTC. Courtesy [16]

- i. Aperture width (W_{apert})
- ii. Aperture length (L_{apert})
- iii. Rim angle (ψ)
- iv. Focal length (f)

For a known length of parabola, complete PTC is defined by inputting two of the other three geometric parameters.

Cross section shape of parabola is determined by rim angle and is defined as the angle between optical axis and the line joining rim trough and convergence or focal point.

For a given aperture length and aperture width, there are two ways to design geometry of PTC with respect to size and shape. One is to trace ideal focal length and the other is to design with respect to optimum rim angle.

Calculation of best suited focal length or rim angle essential to optimize optical performance of parabola collector. It defines spacing that incident reflected irradiation needs to cover to converge at receiver from different cross section parts of parabola as depicted in **Fig.7**

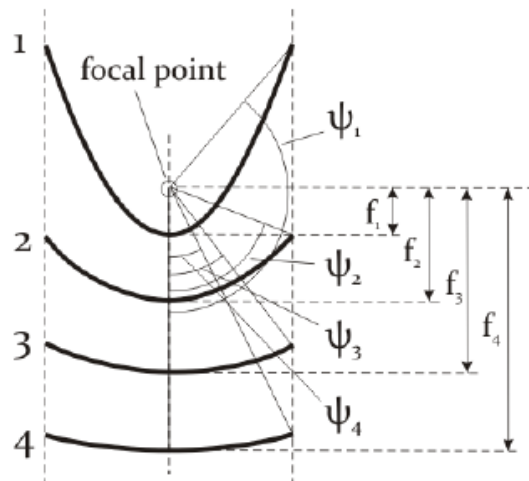


Figure 7: Relationship between focal length and rim angle. Courtesy: [26]

Where

' ψ ' is the rim angle

' f ' represents focal lengths

3.3.1 Concentration ratio

Concentration ratio is another utmost factor which should be considered while calculating appropriate focal length. Reduced focal length normally results in narrow exposed cross section of PTC, while as focal length is increased, it gives broader cross section.

Concentration ratio actually quantifies the amount of solar irradiation focused on receiver tube in comparison to irradiation incident in cross section of parabola. It is calculated by ratio of these two quantities [26].

$$C = \frac{G_{abs}}{G_{aperture}}$$

Where

G_{abs} is Radiant flux density at focal line

$G_{aperture}$ is Beam irradiance at aperture area

It is not easy to calculate these terms. Instead geometric concentration ratio is used for this and is defined as ratio of receiver tube projection area to aperture area [26].

$$C = AREA(abs)/AREA(aperture)$$

$$C = \frac{d}{w}$$

d is diameter of absorber tube

w is aperture width

By this relation concentration ratio for my case study was calculated to be 19.

3.3.2 Tracing Ideal Focal Length:

Focal length depicts how much distance incident reflected rays have to travel to strike receiver tube from different cross sections of the parabola collector. In field real PTC always has some geometric errors like slope inaccuracy. It definitely affects the performance of parabola collector. If there is a slope error, then larger focal length means

larger distance between receiver tube and different collector parts and hence greater loss of reflected irradiation. **Fig.7** shows distance of reflected sun rays from vertex of PTC to focal line amplifies with increase in focal length. While decrease in focal length causes less traveled distance from rim of trough to receiver tube. When optimum focal length has been chosen with respect to given aperture length and aperture width, then it's easy to define PTC in terms of shape and size.

Ideal focal length is chosen by interpolating the equations of focal length involving no slope error and actual focal length having slope errors or misalignment in reflecting mirror. For the absorber tube of known diameter, we will evaluate number of solar rays lost using difference of two focal lengths for different distances and then choose the suitable focal length based on these results.

Optimum focal length for a given aperture width and aperture length was traced by using MATLAB and then it was validated by using design software Parabola calculator 2.0.

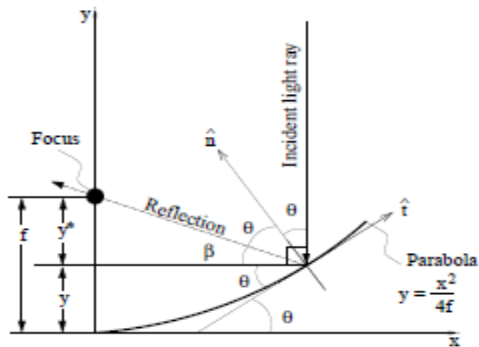


Figure 8.a perfect alignment case
courtesy [17]

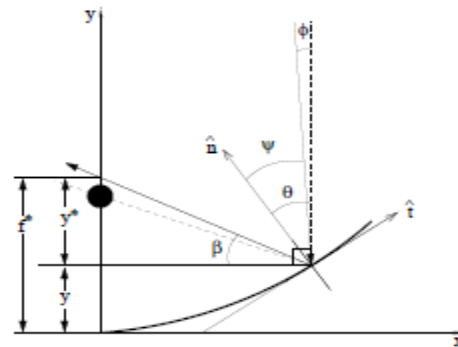


Figure 8.b in case of misalignment Φ

Analytical equations are implemented in MATLAB to calculate ideal focal length for mini PTC. $\tan\theta$ giving slope of the parabola is calculated as [27]

$$\tan \theta = \frac{dy}{dx} = \frac{x}{2f}$$

$$\theta = \tan^{-1} \left(\frac{x}{2f} \right) \text{-----(2)}$$

$$y^* = f^* - y = x * \tan \beta \text{-----(2-a)}$$

$$f^* = x * \tan \beta + y \text{-----(2-b)}$$

We derived difference in focal lengths for the two cases. When there is no slope or misalignment the two focal lengths remain same, while the difference becomes considerable for the second case. Now this difference in focal lengths terms of mathematical equations is calculated using below relations [27]

Now considering **Fig.8a** and **Fig.8b**,

$$\psi = \theta - \Phi$$

$$\beta = \frac{\pi}{2} - \psi - \theta = \frac{\pi}{2} - 2 * \theta + \Phi$$

$$y^* = x * \tan \left(\frac{\pi}{2} - 2 * \theta + \Phi \right) = x * \tan \left[\frac{\pi}{2} - 2 * \tan^{-1} \left(\frac{x}{2f} \right) + \Phi \right] \text{-----(2c)}$$

$$f^* = x * \tan \left[\frac{\pi}{2} - 2 * \tan^{-1} \left(\frac{x}{2f} \right) + \Phi \right] + \frac{x^2}{4*f} \text{-----(2d)}$$

Numerical modeling was done using above mentioned analytical equations in MATLAB using boundary conditions in my case to trace out optimum ideal focal length. For my project specifications of small scale PTC were used with aperture width of 1.6 ft and focal length was varied from 2 inches to 5 inches. No of lost rays were evaluated at each focal length. The optimum ideal focal length for the subject case study was traced to be 4.7 inches. The software parabola calculator 2.0 verified the results of MATLAB model. Complete MATLAB code is provide in soft copy to department.

For the calculated optimum focal length, the no of lost sun rays reached approx. 41% for a misalignment error of 4°. I used this optimum traced focal length of 4.7 inches for the modeled Mini PTC.

IMPLEMENTATION OF NUMERICAL MODEL

4.1 Numerical Modeling for Heat Transfer Analysis (HTA) of PTC

One dimensional steady state energy balance equations are implemented in MATLAB software for numerical modeling of mini PTC. A numerical analysis technique, Newton Raphson method is used for HTA under varying boundary value conditions. Energy flow balance was done on solar collector tubes to determine heat gain by varying different configurations

- i. Perfect evacuated absorber tube
- ii. Lost vacuum absorber tube
- iii. Broken absorber tube

Solar thermal power plants performance is considerably affected by each variation in configuration. In case of any mishap during the operation of solar thermal plants, receiver tubes can lose vacuum or can be broken as shown in **Fig.9**. For cost effectiveness, it becomes very important to quantify how much thermal efficiency has been degraded to help owners when the best time to replace is degraded solar collector receiver for cost effectiveness. Black chrome selective coated receiver tubes have been used to increase the absorptivity and reduce emissivity of absorber tube. Outer glass cover of absorber tube protects it from environmental degradation and significantly reduces thermal losses.

Mathematical modeling of mini PTC is a three step procedure.

- 1) Extraction of meteorological data for experimentation site and calculation of hourly beam irradiation
- 2) Optical modeling of PTC
- 3) Energy balance modeling for absorber tube

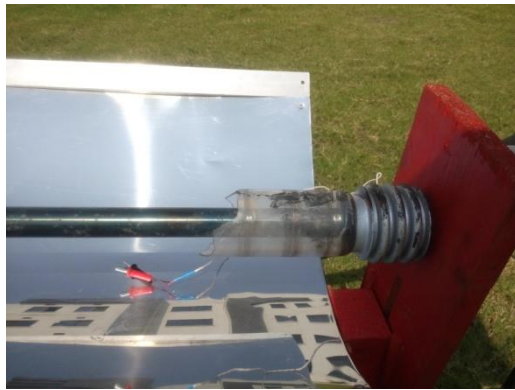


Fig.9a. For Broken



Fig.9b. For Lost Vacuum



Fig.9c. For Perfect vacuum absorber tubes

For first step hourly beam irradiation falling on parabola's aperture area (A_{apert}) was evaluated using meteorological data for SMME, NUST. Then actually solar energy transferred to collector receiver tube was determined by calculating optical efficiency of parabola sheet. For known amount of input energy on receiver tube, HTA was employed. HTA could be 1-D or 2-D depending on receiver tube dimensions. Reasonably accurate results can be obtained using one dimensional HTA for absorber tubes having length less than 100 meter [28]. General algorithm flow chart is shown in Fig.10. Details of the steps are described in following pages.

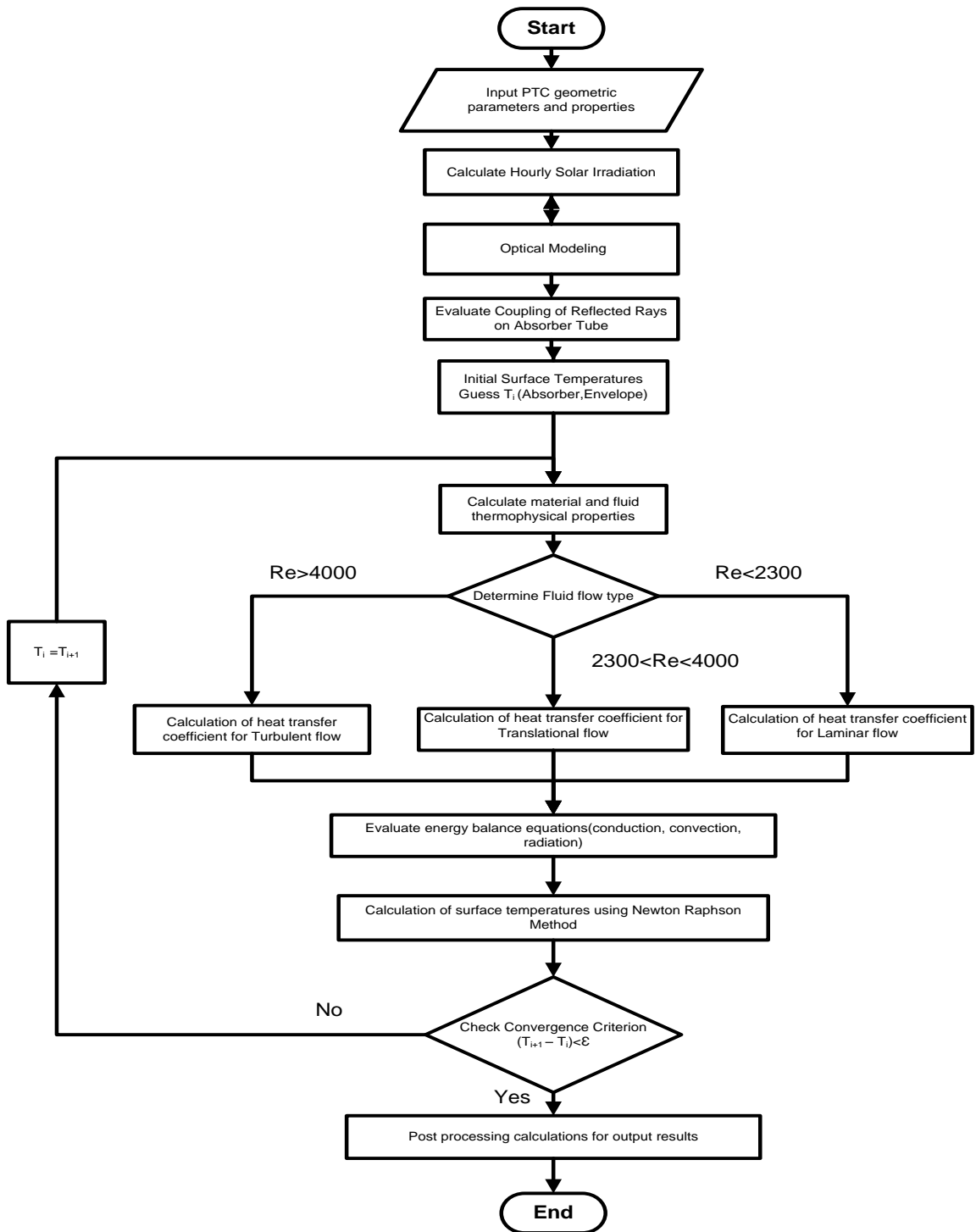


FIG.10. General Algorithm flow chart scheme

4.2 Evaluation of Hourly Irradiation

The climatic data of experimentation site, SMME, NUST having coordinates Latitude: 33.636, Longitude: 72.99 were used [29]. Meteorological data was extracted from **Atmospheric Science Data Centre of NASA and is attached as Appendix-i.** NASA uses data of last 22 years to predict average meteorological data of the required site. Based on monthly diffused, beam and global energy available for the subject site, daily average irradiation was calculated. Required hourly sun irradiation is evaluated by implementing empirical equations representing the curves given by Lui and Jordan in 1960[30].

$$r_t = \frac{\pi}{24} * (a + b * \cos \omega) * \frac{\cos \omega - \cos \omega_s}{\sin \omega_s - \left(\pi * \frac{\omega_s}{180}\right) * \cos \omega_s} \quad \text{-----(3)}$$

Constants a and b are calculated by relations

$$a = 0.409 + 0.5016 * \sin(\omega_s - 60) \text{-----(3a)}$$

$$b = 0.6609 - 0.4767 * \sin(\omega_s - 60) \text{-----(3b)}$$

Global hourly irradiation is obtained by multiplying r_t with Global daily insolation striking any horizontal surface

$$I_t = r_t * H_t \text{-----(3c)}$$

Where

I_t = Global hourly irradiation for horizontal surface.

H_t = the Global daily irradiation for horizontal surface. It is sum of beam radiation and diffused radiation.

ω = Hour angle which is fifteen degree per hour ($15^0 / \text{hr}$) and can be defined as relative angular position of sun and earth along east or west of local meridian. ω is considered positive for afternoon and –ve for morning time.

ω_s = Sun set hour angle and is defined as angular position of sun at sunset time w.r.t to local meridian. Sunset hour angle is given by the relation

$$\omega s = -\tan \Phi \tan \delta \text{-----(3d)}$$

Where Φ is latitude of the selected site which is 33.5 for the current thesis experimentation.

δ = Declination and is angular displacement of sun at noon wrt to equator plane which is $-23.45 \leq \delta \leq 23.45$ [16].

$$\delta = 23.45 * \sin \left(360 * \frac{284+n}{365} \right) \text{-----(3e)}$$

For declination in equation (3e), day number ‘n’ is assigned to each day according to **Table.2** [30].

Similarly from known monthly diffused solar irradiation on horizontal surface, hourly diffused solar irradiation is evaluated using the relations

$$I_d = r_d \times H_d \text{-----(4)}$$

Where r_d is given by

$$r_d = \frac{\pi}{24} * \frac{\cos \omega - \cos \omega s}{\sin \omega s - \left(\pi * \frac{\omega s}{180} \right) * \cos \omega s} \text{-----(4a)}$$

Table.2 Recommended value of n by month [30]

Month	n for ith Day of Month	For the Average Day of the Month		
		Date	n, Day of Year	δ , Declination
January	i	17	17	-20.9
February	31 + i	16	47	-13.0
March	59 + i	16	75	-2.4
April	90 + i	15	105	9.4
May	120 + i	15	135	18.8
June	151 + i	11	162	23.1
July	181 + i	17	198	21.2
August	212 + i	16	228	13.5
September	243 + i	15	258	2.2
October	273 + i	15	288	-9.6
November	304 + i	14	318	-18.9
December	334 + i	10	344	-23.0

I_b can be found by subtracting I_d and I_t .

From calculated I_d and I_t values, I_b can be evaluated by the relation

$$I_b = I_t - I_d$$

Where

I_d = diffused hourly irradiation data

I_t = Global hourly irradiation data

I_b = Beam or direct hourly irradiation

4.3 Optical Model of PTC

Optical performance of PTC depicts how much sun energy is transferred to absorber tube. Optical efficiency of parabola collector is directly affected by many parameters and is calculated by considering error terms. Error terms influencing the optical efficiency of PTC includes geometric misalignment error which has been described in earlier section 4.3 of geometry design of PTC, sun tracking errors, reflectivity properties of parabola reflecting sheet, Dust factors for reflecting sheet and receiver tube and sun energy losses due to shadow effect on PTC.

The Computational optical model is used to calculates optical efficiency of parabolic trough collector by taking into consideration error terms as shown in **Table-3**[31]

Table-3. Error terms considered in optical modeling

ϵ_1 =Shadow Effect on PTC	0.98
ϵ_2 = Error due to sun tracking	0.92
ϵ_3 =Geometric alignment error	0.87
ϵ_4 =Dust on Reflecting mirror	Reflectance/ ρ_{cl}
ϵ_5 =Dust on receiver tube	$(1 + \epsilon_4)/2$
ϵ_6 =Miscellaneous errors	0.96
ρ_{cl} =Reflectivity of Clean mirror sheet	0.93

All error factors are combined to evaluate the optical efficiency of PTC.

$$\eta_{optical} = \epsilon_1 \epsilon_2 \epsilon_3 \epsilon_4 \epsilon_5 \epsilon_6 \rho_{cl} K \text{ -----(5)}$$

Where as

ϵ_1 presents error occurred due to shadow on receiver tube and it was considered to be 0.98 in my case.

ϵ_2 gives modifying error term used to consider due to sun tracking. For our model it is considered to be 0.92. The PTC equipped with manual tracing system and therefore errors can be larger.

ϵ_3 represents error occurring due to geometric fabrication misalignment of PTC system. In commercial scale production for larger project, the precision of manufacturing processes of PTC is very precise and hence low misalignment errors. While for my project due to unavailability of precise fabrication resources, the error induced was relatively larger than optical tracing of sun rays along the focal length and for my model it was considered about 0.87.

ϵ_4 gives the error term to account losses due to dust particles on parabola reflecting sheet and is given by relation Reflectance / ρ_{cl} .

ϵ_5 gives error used to account for dust/dirt on receiver tube and is calculated by $(1 + \epsilon_4)/2$

ϵ_6 is a modified term error used to cater for unaccounted miscellaneous losses.

ρ_{cl} represents clean mirror reflectivity. For the subject experimental study due to unavailability of appropriate reflecting sheet for PTC like Miro-4, I had to go for economical reflecting sheet that is stainless steel and for my model it was considered to be 0.93

When solar radiation is not incident normal to the aperture area incident angle modifier (K) comes into play and is a function of incidence angle. Following relation for Incident angle modifier in Equation-(1) is used [13]

$$K = \cos(\theta) + 0.000884(\theta) - 0.00005369(\theta^2) \text{ ----- (6)}$$

Where θ is the incident angle and is defined as angle made by solar beam rays on the reflecting surface with the normal of surface [30]

4.3.1 Solar Energy Absorbed by Receiver Glass Envelope

To simplify the computational model, sun energy absorbed by glass envelope is considered as heat flux. This is because the thickness of glass envelope is very small and absorptance coefficient is minimal about 0.02 [32]. Optical efficiency of absorber glass envelope is calculated to determine the solar energy absorption by the relation

$$\dot{Q}'_{5solabs} = \dot{Q}'_{si} \eta_{env} \alpha_{env} \text{ -----(7)}$$

$$\eta_{env} = \epsilon_1 \epsilon_2 \epsilon_3 \epsilon_4 \epsilon_5 \epsilon_6 \rho_{cl} K \text{ -----(7a)}$$

$$\dot{Q}'_{si} = \frac{I_b A_{apert}}{L_{apert}} \text{ -----(7b)}$$

Where

$\dot{Q}'_{5solabs}$ is solar irradiance absorption in glass envelope

η_{env} is optical efficiency of glass envelope

α_{env} is absorptivity of receiver glass envelope

\dot{Q}'_{si} is incident solar irradiation per length of receiver tube (W/m).

I_b is direct irradiance in W/m

L_{apert} is aperture length of parabola collector

K is incidence angle modifier as described earlier

4.3.2 Solar irradiance absorption in absorber tube

Solar energy absorption on coated surface of absorber tube is a surface phenomenon and is considered uniform heat flux. Solar irradiance absorption in absorber is governed by following equations

$$\dot{Q}'_{3solabs} = \dot{Q}'_{si} \eta_{abs} \alpha_{abs} \text{ -----(8)}$$

$$\eta_{abs} = \eta_{env} \tau_{env} \text{ -----(8a)}$$

where

$\dot{Q}'_{3solabs}$ is solar irradiance absorbed by absorber surface (W/m)

η_{abs} is absorber surface optical efficiency

α_{abs} is absorber absorptance

τ_{env} is transmittance of receiver glass cover

4.4 Energy Balance Model of Absorber Tube

The energy balance model used for heat transfer analysis of absorber tube uses steady state energy balance equations between heat transfer fluid (HTF) and ambient atmosphere. The model uses all equation and mathematical correlations required to evaluate the parameters for energy balancing. It directly depends on collector type, absorber tube configuration and boundary value conditions. The computational model evaluates performance of PTC by using three different configurations of solar absorber tube as shown in **Fig.9**

1. Perfect vacuum solar absorber tube with annulus between receiver surface and the envelope.

2. Lost vacuum absorber tube having air breached into annulus but glass envelope is intact.
3. Broken receiver tube having no envelope and absorber is directly exposed to ambient atmosphere.

Energy balance model works by conserving energy at each end of receiver tube. 1-D steady state energy balance model for the discussed three configurations of solar absorber tube is shown in **Fig.11**. The equivalent thermal resistance model for the subject cases is shown in **Fig.12**. To simplify incident sun energy and optical losses are not mentioned in resistance model.

A part of incident sun energy which is solar irradiance multiplied with optical efficiency) on focal line is absorbed by glass envelope ($\dot{Q}'_{5solabs}$) and remaining by selective coated absorber surface ($\dot{Q}'_{3solabs}$). Major part of energy absorbed by chrome coated surface is conducted (\dot{Q}'_{23cond}) and transferred to heat transfer fluid (water) by convection (\dot{Q}'_{12conv}); remaining portion of sun energy is lost to glass cover through convection (\dot{Q}'_{34conv}) and radiation(\dot{Q}'_{34rad}). The amount of energy conducted (\dot{Q}'_{45cond}) by glass envelope plus already absorbed energy ($\dot{Q}'_{5solabs}$) is lost to atmosphere mostly by convection (\dot{Q}'_{56conv}) and to some extent by radiation (\dot{Q}'_{57rad}). For broken absorber tube where glass envelope is not present, absorber tube surface is directly exposed to atmosphere and thermal energy losses extensive and direct to atmosphere. Assumptions and boundary conditions of energy model are described in section 4.6.

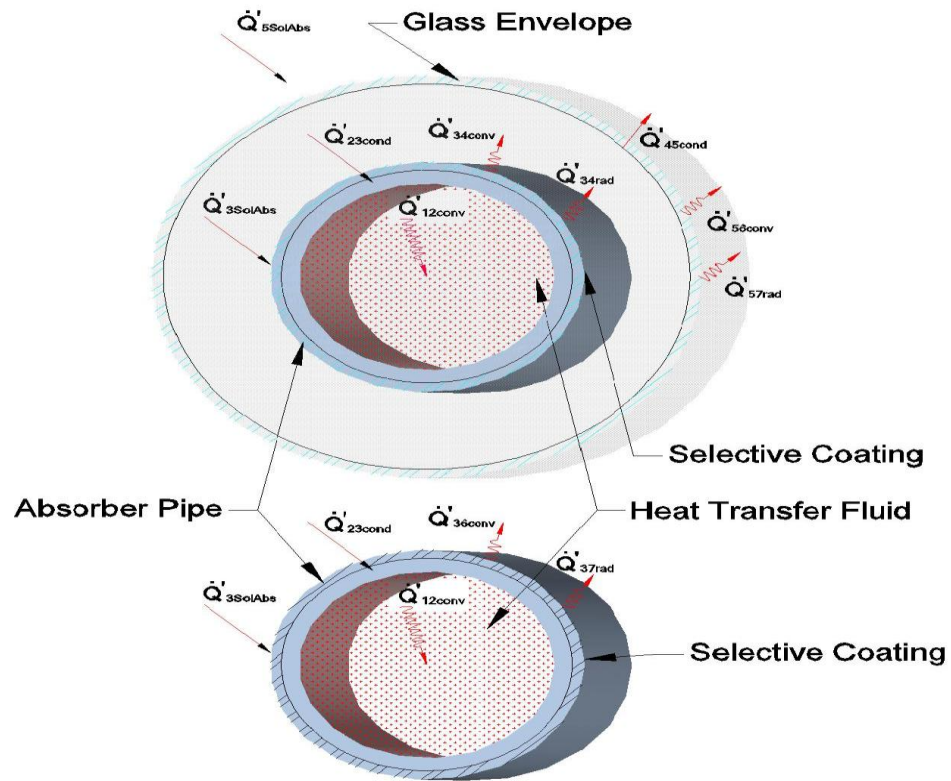


Fig.11 1-D steady state energy balance model (a) For evacuated and lost vacuum receiver configuration (b) For Broken glass configuration

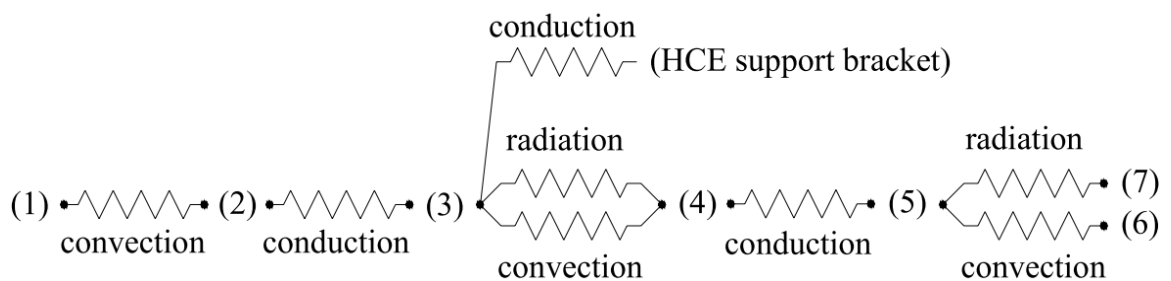


Fig.12 Equivalent thermal resistance model. Courtesy [24]

Where in **Fig.11** for thermal resistance model

- (1) = HTF (water)
- (2) = Inner surface of absorber receiver

- (3) = Outer surface of absorber receiver
- (4) = Inner Surface of glass cover
- (5) = Outer Surface of glass cover
- (6) = surrounding atmosphere
- (7) = Sky

Energy balance equations for the model are derived by conserving energy at each end as indicated in **Fig-11**. For perfect vacuum absorber tube and lost vacuum solar absorber tubes, the governed energy balance equations are

$$\dot{Q}'_{12conv} = \dot{Q}'_{23cond} \text{-----(9)}$$

$$\dot{Q}'_{3solabs} = \dot{Q}'_{34conv} + \dot{Q}'_{34rad} + \dot{Q}'_{23cond} \text{-----(9a)}$$

$$\dot{Q}'_{45cond} = \dot{Q}'_{34conv} + \dot{Q}'_{34rad} \text{-----(9b)}$$

$$\dot{Q}'_{5solabs} + \dot{Q}'_{45cond} = \dot{Q}'_{56conv} + \dot{Q}'_{57rad} \text{-----(9c)}$$

$$\dot{Q}'_{Heatloss} = \dot{Q}'_{56conv} + \dot{Q}'_{57rad} \text{-----(9d)}$$

And for broken solar absorber tube

$$\dot{Q}'_{12conv} = \dot{Q}'_{23cond} \text{-----(9e)}$$

$$\dot{Q}'_{3solabs} = \dot{Q}'_{36conv} + \dot{Q}'_{37rad} \text{-----(9f)}$$

$$\dot{Q}'_{Heatloss} = \dot{Q}'_{36conv} + \dot{Q}'_{37rad} \text{-----(9g)}$$

4.4.1 Heat Energy Transfer from Absorber Surface to HTF by Convection (\dot{Q}_{12conv})

Thermal energy is transferred from inner surface of absorber tube to heat transfer fluid (Water) by convection and is given by Newton's law of cooling

$$\dot{Q}_{12conv} = h_1 D_1 \pi (T_2 - T_1) \text{-----(10)}$$

$$h_1 = Nu_{D_1} \frac{K_1}{D_1} \text{-----(10a)}$$

Where

h_1 is heat transfer coefficient of HTF at the temperature of T_1 (W/m²-K)

D_1 Absorber inside diameter (m)

T_1 Inlet HTF temperature (K)

T_2 Receiver inside surface temperature (K)

Nu_{D_1} Nusselt number based on D_1

K_1 Thermal conductivity of the HTF at T_1 (W/m-K)

4.4.1.1 Flow cases for HTF within absorber tube

The computational model contains conditions to evaluate the flow type in HCE and Nusselt number (Nu) depends on nature of flow. For the subject model the flow is mostly laminar or translational due to viscosity of water at low operating temperatures and low flow rate. Therefore thermal energy losses and heat gain are affected by flow type.

4.4.1.2 Turbulent & Translational Flow Conditions

Type of flow condition depends on Reynolds number. For translational flow Reynolds no remains between 2300 and 4000. For Reynolds number greater than 4000, the flow turn into turbulent. This conditional flow is determined by Gnielinski correlation [37]

$$Nu_{D_1} = \frac{f/8 (Re_{D_1} - 1000) Pr_1}{1 + 12.7 \sqrt{f/8} (Pr_1^{2/3} - 1)} \left(\frac{Pr_1}{Pr_2} \right)^{0.11} \text{-----(10b)}$$

$$f = (1.82 \log_{10}(Re_{D_1}) - 1.64)^{-2} \text{-----(10c)}$$

Where

Pr_1 Prandtl number of water at T_1

Pr_2 Prandtl number of water at T_2

f friction factor for absorber surface

Gnielinsky correlation is applicable for prandtl Nos between 0.5 and 2000 and for Reynolds No between 3000 & 5×10^6 [34].

4.4.1.3 Laminar Flow

For Reynolds number range less than 2300, the flow is laminar type and Nusselt No has a constant value of 4.36[34]

4.4.2 Heat Energy Transfer across Absorber by Conduction (\dot{Q}_{23cond})

Conduction heat transfer through absorber wall is given by Fourier's law of conduction [34]

$$\dot{Q}_{23cond} = 2\pi K_{23} (T_2 - T_3) / \ln \left(\frac{D_2}{D_1} \right) \text{-----(10d)}$$

Where

T_3 Receiver outside surface temperature (K)

D_2 Absorber outside diameter (m)

K_{23} Thermal conductivity of absorber at T_{23} (W/m-K)

4.4.3 Heat Energy Transfer from Absorber Surface to Glass Cover

Thermal Energy transfer from absorber surface to glass envelope surface involves radiation and convection mechanisms. Heat transfer by convection depends on pressure and condition of vacuum in annulus [35]. Difference in temperature between outer absorber surface and inner surface of Glass cover results in radiation heat transfer. The envelope made-up of glass is assumed to be opaque to IR for radiation heat transfer and gray surfaces are assumed.

4.4.3.1 Heat Transfer by Convection (\dot{Q}_{34conv})

Convection heat transfer can be by free molecular or natural convection depending upon whether the receiver tube is working under perfect vacuum at low pressure or breached vacuum at atmospheric pressure.

4.4.3.2 For Perfect Vacuum Absorber Tube

For evacuated absorber tube pressure inside annulus is considered at low pressure. For low pressure in annulus at $< \sim 1$ torr, heat energy transfer occurs by free molecular convection [36]. It is given by equation

$$\dot{Q}_{34conv} = h_{34} D_2 \pi (T_3 - T_4) \text{-----(11)}$$

$$h_{34} = \frac{K_{std}}{(D_2/2 \ln(D_3/D_2) + b\lambda(D_2/D_3 + 1))} \text{-----(11a)}$$

$$b = \frac{(2-a)(9\gamma-5)}{2a(\gamma+1)} \text{-----(11b)}$$

$$\lambda = \frac{2.331E(-20)(T_{34} + 273.15)}{(P_a \delta^2)} \text{-----(11c)}$$

Where as

D_3 inner glass envelope diameter (m)

D_4 Outer diameter of glass covering (m)

h_{34} heat transfer coefficient by convection for gas at T_{34} (W/m²-K)

T_4 Inside envelope surface temperature (K)

K_{std} Thermal conductivity for annulus gas at STP (W/m-K)

b interaction coefficient

a accommodation coefficient

λ Mean-free-path for a molecule (cm)

γ Ratio of specific heats for the annulus gas

T_{34} average temperature $(T_3 + T_4)/2$ (K)

δ Molecular diameter (cm)

P_a Annulus pressure (mmHg)

4.4.3.3 For Lost Vacuum Absorber Tube

When vacuum inside annulus is lost due to environmental degradation, pressure inside the absorber tube increases (pressure > ~1 torr) and heat energy transfer occurs by natural convection. For natural convection heat energy transfer in annulus space Raithby & Holland derived following relation [37]

$$\dot{Q}_{34conv} = \frac{2.425 K_{34} (T_3 - T_4) (Pr Ra_{D_2} / (0.861 + Pr_{34}))^{1/4}}{(1 + (D_2 / D_3)^{3/5})^{5/4}} \text{-----(12)}$$

$$Ra_{D_2} = \frac{g \beta (T_3 - T_4) D_3^3}{\alpha \nu} \text{-----(12a)}$$

Where as

K_{34} Thermal conductivity of vacuum gas in annulus at T_{34} (W/m-K)

Pr_{34} Prandtl number of air at T_{34}

Ra_{D_2} Rayleigh number at D_2

β Volumetric thermal expansion coefficient (1/K)

4.4.3.4 Heat Energy Transfer by Radiation (\dot{Q}_{34rad})

Following relation is used to evaluated heat energy transfer by radiation from absorber surface to glass envelope [34]

$$\dot{Q}_{34rad} = \frac{\sigma \pi D_2 (T_3^4 - T_4^4)}{(1/\varepsilon_3 + (1 - \varepsilon_4) D_2 / \varepsilon_4 D_3)} \text{-----(13)}$$

Where as

σ Stefan-Boltzmann constant (W/m²-K⁴)

ε_3 Emissivity of receiver selective coating

ε_4 Emissivity of glass envelope

4.4.4 Heat Energy Transfer through Glass Envelope by Conduction (\dot{Q}_{45cond})

Conduction through envelope surface is governed by Fourier law of heat transfer [34] by same relation as used for conduction through absorber surface.

$$\dot{Q}_{45cond} = 2\pi K_{45} (T_4 - T_5) / \ln \left(\frac{D_4}{D_3} \right) \text{-----(14)}$$

Where as

K_{45} Thermal conductivity of vacuum gas at T_{45} (W/m-K)

T_5 Envelope Surface outside temperature (K)

4.4.5 Heat transmission from Envelope Surface to Atmosphere

The amount of thermal losses from receiver tube is predicted by heat energy transfer from receiver outer surface to atmosphere. For first two configurations, heat energy transfer occurs from glass envelope surface to atmosphere while for broken absorber tube case, heat transfer occurs directly from absorber surface to atmosphere. Heat transfer to atmosphere is mostly by convection and some by radiation depending on wind speed.

4.4.5.1 Heat Energy Transfer by Convection (\dot{Q}_{56conv})

Convection heat energy transfer can be natural or forced depending on wind speed. Majority of heat energy losses from glass envelope to atmosphere are by convection and

it even becomes significant when high speed wind is blowing. In the subject study, for Islamabad climatic conditions wind speed is normally high. So forced convection heat energy transfer is given by Newton's law of cooling

$$\dot{Q}_{56conv} = h_{56}\pi D_4(T_5 - T_6) \text{-----(15)}$$

$$h_{56} = \frac{K_{56}}{D_4} Nu_{D_4} \text{-----(15a)}$$

Where as

T_6 Ambient Temperature (K)

h_{56} Convection thermal coefficient for air at T_{56} (W/m²-K)

K_{56} Thermal conductivity of air at $(T_5 - T_6)/2$ (W/m-K)

Nu_{D_4} Nusselt number based on D_4

Nusselt number (Nu_{D_4}) depends on wind speed. For forced convection where wind flow is normal to isothermal cylinder, nusselt number is calculated using Zhukauskas' correlation [34]

$$Nu_{D_4} = C Re_{D_4}^m Pr_6^n \left(\frac{Pr_6}{Pr_5} \right)^{1/4} \text{-----(15b)}$$

Where values of C and m for different ranges of Reynolds number are given by **Table-4**

Table-4 Corresponding values of C & m to Reynolds no

Re	C	m
200000-1000000	0.076	0.7
1000-200000	0.26	0.6
40-1000	0.51	0.5
1-40	0.75	0.4

For $Pr \leq 10$, $n=0.37$ & For $Pr > 10$, $n=0.36$

Where as

Pr_6 Prandtl number of open air at T_6

Pr_5 Prandtl number of open air at T_5

Re_{D4} Reynolds number based on D_4

4.4.5.2 Heat Energy Transfer by Radiation (\dot{Q}_{57rad})

Radiation heat losses from glass envelope surface to atmosphere are due to temperature difference b/w envelope surface and sky. For this glass envelope is considered gray object surrounded by black body (sky). Radiation heat energy transfer is given by [34]

$$\dot{Q}_{57rad} = \sigma \pi \epsilon_s D_4 (T_5^4 - T_7^4) \text{ -----(16)}$$

Where as

σ Stefan-Boltzmann constant ($W/m^2 \cdot K^4$) ($5.670E-8$)

T_7 Effective sky temperature (K)

4.4.6 Heat Energy Transmission for Broken Glass tube

For broken absorber tube when envelope is missing, heat energy transfer to atmosphere are direct and losses become prominent as compared to first two configurations of receiver tube. For this case radiation and convection heat losses are calculated by same relations as given in section 4.4.5. Solar absorption ($\dot{Q}_{3solabs}$) as previously calculated in optical model is adjusted for solar energy which is not lost glass envelope for this case.

4.5 Implementation of Numerical Modeling in MATLAB

Previously described mathematical model for mini PTC is implemented in MATLAB Software. The code of Main MATLAB program along with integrated functions is provided in soft form. One dimensional steady state Energy balance equations and optical model equations are applied for three different cases of absorber collector tubes to govern partial differential equations evaluating the performance of PTC in each case for the simulation model.

Numerical analysis technique using Newton Raphson method is used to implement optical and energy balance model of PTC using MATLAB coding. The performance of PTC has been evaluated by varying different parameters and boundary value conditions for three different configurations of absorber tube as described earlier. For each absorber receiver case one dimensional steady state energy balance equations were employed b/w surrounding atmosphere and working fluid (water) to determine performance of PTC by varying different parameters. The implemented model delivers reasonably true results for smaller receiver of less than 100 m for parametric comparison study [28]

Derived partial differential equations of numerical model are employed using root finding algorithm technique. Working fluid in hydraulic scheme remains single phase as experimentation was performed using small scale PTC which receives low amount of solar energy. Analytically derived algebraic equations from the subject model contain unknown surface temperatures (T_2 , T_3 , T_4 , and T_5). Known heat fluxes are integrated in derived equations and then solved numerically by taking initial guess of surface unknown temperatures. Incident sun energy reflected from parabola sheet on absorber surface is a function of optical model of PTC. For known initial conditions at the inlet segment and boundary condition at absorber wall, implemented one dimensional energy model evaluates surface temperatures of receiver tube and then using these values performance of PTC is determined.

Flow chart scheme of general algorithm implemented in MATLAB for HTA for the considered three cases of HCE (Heat collector element) is shown in **Fig-11**. The calculation of algorithm for the computational model is a three step process;

1. Pre processing calculation of hourly direct solar irradiance
2. Calculation of energy incident on absorber tube based on optical model
3. Implementation of 1-D energy balance model for HTA

The optical model determines the amount energy focused on receiver tube and energy balance modeling is initiated with initial guess of unknown temperatures. The model calculates material properties as per heat fluxes and surrounding conditions. Numerical

analysis technique is then employed for by coupling steady state energy balance equations and loop runs successive iterations until error convergence criterion is met. Global error convergence is approached when error difference of consecutive iterations become constant and verifies the global convergence criterion $T_{i+1} - T_i < \text{error}$. Whereas $\text{error} < 10^{-5}$.

The numerical model evaluates the comparative performance of PTC by varying following operating parameters for three considered cases of receiver tubes

- HTF inlet temperature (T_1)
- Flow rate of HTF (\dot{M})
- wind velocity (W_v),
- ambient temperature (T_{amb}),
- Aperture Area (A_{apert})
- Receiver diameter (D_1)

Comparative performance of PTC is evaluated by calculating outlet temperature, heat loss, heat gain and efficiency.

4.6 Boundary Conditions

Table-5 shows operational conditions and specifications of modeled PTC. Considered error terms for the calculation of effective optical efficiency of reflecting sheet are mentioned in **Table-3**. Same optical properties are assumed for all three configurations. All the thermodynamic properties, heat fluxes and temperatures are considered as uniform along the length and around perimeter of HCE. Positive direction of heat fluxes is shown in **Fig.11**. Algebraic equations are derived in energy balance model by considering conservation of heat energy at collecting section for the considered three configurations of receiver tube. Material properties of receiver tubes like absorptance, emittance and transmittance are taken constant (As provided by manufacturer) and independent of surrounding temperature. Conduction through support brackets of PTC is neglected as being made up of wooden material. Radiation heat energy losses to atmosphere assume that absorber tube surface is a small gray body which is surrounded by huge black body, the sky.

Table-5 Specifications of PTC

Date: 6 September 2014

Time: 1200hrs to 1300 hrs

Latitude = 33.636

Longitude = 72.99

$D_1 = 0.024$ m

$D_2 = 0.0254$ m

$D_3 = .050$ m

$D_4 = .058$ m

$T_6 = 312$ K

$T_7 = T_7 - 8$ K

$L_{apert} = 1.8$ m

$W_{apert} =$

$I_b = 905$ W/m²

$\alpha_{env} = 0.02$

$\varepsilon_3 = 0.86$

$\alpha_{abs} = 0.94$

$\tau_{env} = 0.935$

$T_1 = 310:1:340$

$\dot{m} = .07:0.01:0.37$ kg/sec

$A_{apert} = 1: 0.2 :3$ m²

$W_v = 0.1 : 0.1: 2.5$ m/sec

$T_{amb} = 300: 2 :322$ K

FABRICATION FOR EXPERIMENTATION SETUP OF PTC

5.1 Fabrication Process

Fabrication of parabolic trough collector requires high degree of precision in its manufacturing. As discussed earlier in designing section, a little misalignment error while fabricating parts of PTC can lead to high optical losses and hence low thermal efficiency. Due financial constraints small scale model was fabricated for experimentation. PTC was fabricated using manufacturing resource facility (MRC) at SMME, NUST. Detail of each manufactured part is provided in following sections

5.2 Parabola Reflecting Sheet

Amount of energy focused on absorber pipe is directly affected by reflectivity of parabola mirror. High reflectivity material such as Miro-4 has very high reflectivity but the material is not available and is costly to import. Due to easy availability and high reflectivity stainless steel sheet of 28 gauges is used for mini PTC. Size of the selected sheet was 5.9 x 2.6 (ft x ft). Special care was taken for bending and while putting in place stainless parabola sheet. Ribs made up of wood were used to bend stainless steel sheet as shown in **fig.13** and then screws and side rails were used to fix the sheet in wooden ribs.



Fig.13 Reflecting sheet with parabola ribs for PTC

5.3 Side Rails

Side rails were used to keep parabola sheet in position by attaching it to both ends of wooden ribs. For this purpose light weight angle aluminum of 1.25 x 1.25 (inch x inch) was used. The lengths are attached to wooden ribs as shown in **Fig.14**



Fig.14 Fixing of side rails with wooden ribs along parabola sheet

5.4 Parabolic Ribs

Parabolic ribs are required to support and keep parabola shape of reflecting sheet used in PTC. Ribs are responsible to maintain the parabola shape which is very important factor to achieve focal line with high accuracy. Little misalignment in parabolic shape of ribs could adversely affect the performance of PTC. So this task demanded high precision and accuracy. CNC machine available at MRC was used for this purpose. Mathematical equations in the form of G & M codes were fed into CNC machine to control the cutting and shaping of parabola ribs. Prototype of mild steel was developed by using dimensions shown in **fig.15** that is 3 x 1.5 (ft x ft) rectangular sheet with thickness of 3/8 inches. Holes were created in ribs for fastening and easy marking.

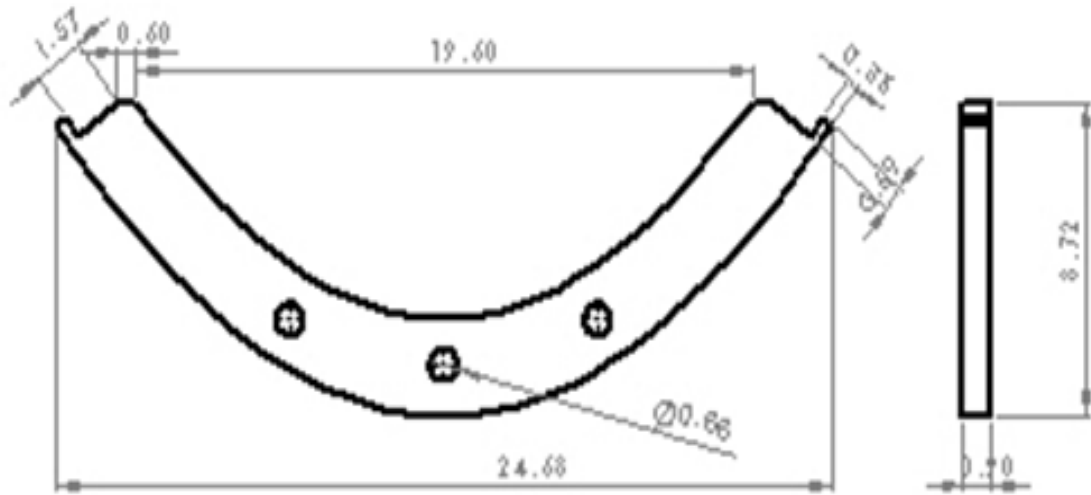


Fig.15 Dimensions of Parabola ribs in inches



Fig.16 (a) Ready parabolic Rib



Fig.16 (b) CNC machine used for parabola ribs

For mini PTC metallic rib was considered as template while all other ribs to be used in PTC were made of wooden material. Marking was done by placing mild steel template on wood and parabolic shape was precisely traced. 12 wooden ribs were made in the process with great care as all ribs needed to be very identical. After fine finishing all twelve wooden ribs were matched check similarity. Tolerance error of 1mm was present but it was acceptable.



Fig.17 Precise fabrication of wooden ribs for PTC

5.5 Support Brackets for Receiver Tube

Precise positioning of solar absorber tube at traced focal length is very important to avoid loss of solar reflected rays. Bearings were used on both fixing ends of receiver as PTC rotates during sun tracking along focus receiver pipe. Inner radius of used bearings is 17.5mm. Bushes were also used in press fittings with bearings to provide strength for holding absorber tubes. Bearings along with bushes were fixed in wood with press fittings as shown in **Fig. 18**. Side support wooden blocks were fastened with parabola ribs by using bolts of 3 inch each.



Fig.18 Fixing of bearings in wood

Absorber receivers of three different configurations but of same manufacturer were used. Absorber tube with inside diameter of absorber pipe is 1 inch. The length of all three absorber tubes is 1.8 meter. Being product of same manufacturer, all three absorber tube surfaces has same selective coating of same emissivity.

5.6 Fabrication of Manual Tracking System for PTC

Tracking assembly is very necessary for PTC system. Normally single axis sun tracking is used for parabolic trough collector systems. For the subject experimentation purpose single axis sun tracking assembly was fabricated, which could be driven manually.

Manually drive assembly was fabricated using simple design consisting of following three major parts as shown in **Fig.19**

- I. Drive arm
- II. Power screw
- III. Control rod

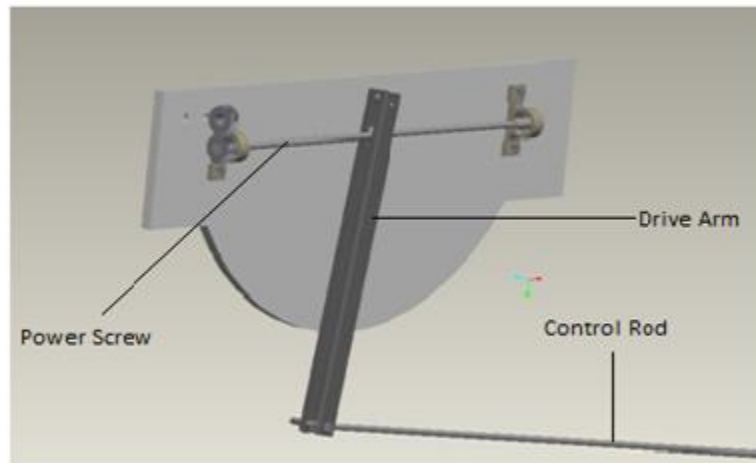


Fig.19 Manual Tracking Drive Assembly

The designed assembly works by moving drive arm as a result of rotation of power screw pivoted as one end. The drive arm intern is connected to control rod. The movement of drive control rod rotates PTC system about sun path in alignment with the rotation of power screw. Components of sun tracking drive assembly are described below

5.6.1 Power Screw

Special care was taken while designing of power screw of drive assembly as it determined the control of tracking mechanism. Power screw design depends on two main factors

- I. Thrust force of power screw
- II. Linear velocity of nut

Pitch of screw was determined by using its rpm and linear velocity. Raising and lowering torques were determined by using thrust to be provided by power screw. The main design challenge of drive assembly was to rotate PTC from $+60^{\circ}$ to -60° from vertical rotation of parabola sheet with angular velocity of 15° per Hour while keeping low torque and rpm to lower value of 8 rpm.

5.6.2 Drive arm

Two drive arms are used with spacing between them for sliding over 02 bearings on axle nut. The used drive arms are 0.61 x .04 (m x m) with .006m bending each. Due to easy availability and low load mild steel was used. On each end of drive arm a 10 mm hole was made. Drive arm becomes a channel with translational motion of axle nut as shown in **Fig-20**



Fig.20 Drive Arm with Axle nut

5.6.3 Control rod

PTC is connected to drive arm through control rod. 6 ft long control rod of mild steel was used with a diameter of 10mm. One threaded end of the rod is attached to yoke of 10 mm diameter and the other end is connected to parabola system through hook. PTC system rotates with the same angle as drive arm.

5.6.4 Bracket Bearings:

Two bracket bearings were used to keep in position power screw drive and to give angular motion as shown in **fig-21**. Pair of bracket bearings was fixed on wooden board as shown in **fig-23b**.



Fig.21 Bracket Bearing

5.6.5 Axle nut

The purpose of axle nut is to convert rotational motion of drive arm into translational movement with the help of control rod. It provides flexibility to the drive arm to revolve around pivoted reference on wooden board. The outer and inner diam of axle nut are 23 mm and 12 mm respectively as shown in Fig.22. The inner surface of axle nut is threaded. Bearings at both ends of 20 mm diameter each allow easy frictionless motion in drive arm.



Fig.22 Axle Nut

5.6.6 Wooden Base

The whole tracking drive assembly was fixed on a wooden base made-up of chip board. Wooden sheet was cut into parabola sheet at lower end as shown in **Fig.23a**. The whole assembly on wooden board looked like as in **Fig.23b** Reason for this shape was easy marking of angles on board. Drilling was done at the centre of wooden board at 21 inches which was also taken as reference point for all angles.



(a)



(b)

Fig.23 (a) Wooden Base (b) Tracking Assembly Mounted on Wooden Base

5.7 Hydraulic Scheme

Hydraulic scheme was designed and implemented as shown in **fig24**. And then plumbing and piping fabrication was done as per requirements in hydraulic design. In order to avoid thermal losses, proper insulation of the parts was done and extensive leakage tests were performed for the designed hydraulic scheme before starting experimentation.

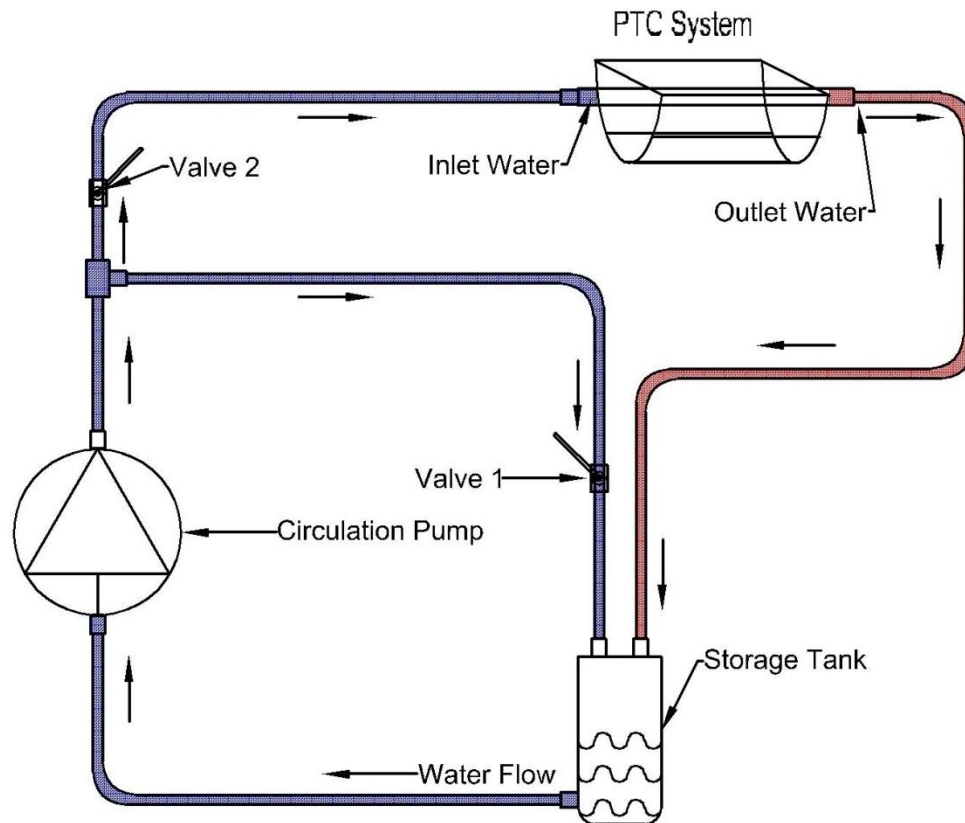


Fig.24 Hydraulic Scheme

Following main components were used in implemented hydraulic scheme as shown in **fig-25**.

- Glass wool Insulated Storage Tank of 10 liter capacity
- Glass wool Insulated Pipe of one inch diameter
- Valves to control water flow rate
- T-Joints
- Circulation pump with variable flow rates



Fig.25 Hydraulic Scheme Used for PTC Experimentation

5.8 Experimentation and Instrumentation

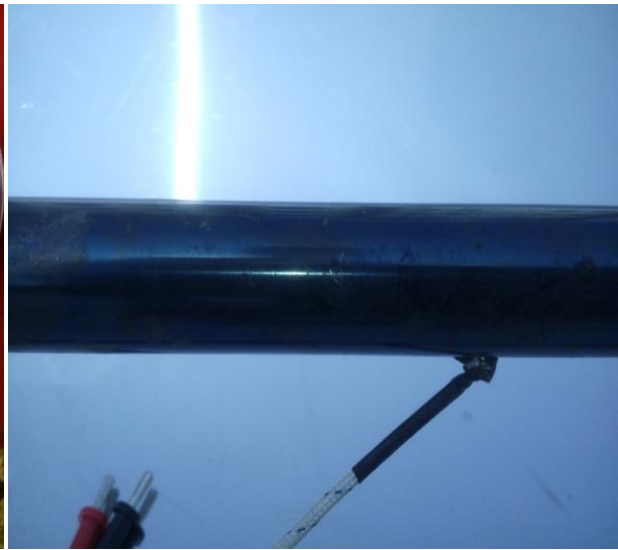
In order to validate simulation results, extensive experimentation was performed using fabricated PTC system and designed hydraulic scheme as described earlier. Following tools were used to measure experimental data

5.8.1 Thermocouple

In experimentation thermocouples were used to measure inlet temperature, outlet temperature and surface temperatures of absorber tube. Thermocouples were attached very carefully to make sure proper measuring of temperature as shown in **Fig.26**



(a)



(b)



(c)



(d)

Fig.26.Placement of thermocouple (a) Glass envelope surface (b) Absorber surface (c) At water inlet (d) At water outlet

5.8.2 Laser thermal gun

Surface temperature measurement of absorber tube with envelope was not possible to measure using thermocouple, for this purpose laser thermal gun was used as shown in

fig-27. Measurement error of thermal gun was evaluated earlier by comparing its reading with thermocouple for broken absorber surface.



Fig.27 Absorber surface temperature measurement using thermal laser gun

5.8.3 Pyranometer

Pyranometer is used to measure real-time solar irradiance on a plane surface. It gives reading in milli volts (mV) on digital millimeter (DMM), which is then converted to watt per meter square (W/m^2) by multiplying with constant.



Fig.28 Solar Irradiance measurement using Pyranometer



Fig. 29 Experimental Setup of PTC along with Manual Tracing System

CHAPTER 6

RESULTS & DISCUSSIONS

Comparative parametric study was done by varying one of the parameters and then analyzes its effect on the performance of PTC graphically for three different cases of absorber tubes under meteorological conditions of Islamabad. Comparative heat transfer study of results reveal the parameters which influence the most on desired output results of PTC system like Output temperature, Heat gain, Heat loss and Efficiency. First simulation results were analyzed to see the affect of varying operating conditions on output results and then these results were verified experimentally for two parameters that is Inlet temperature (T_1) and Mass flow rate (\dot{M}). Comparative simulated and experimental results are in close coherence with negligible error difference. Under similar meteorological conditions efficiency of PTC with perfect vacuum absorber tube is superior to other two configurations of absorber tube i.e. lost vacuum tube and broken absorber tube. This is because thermal losses of broken receiver tube are maximum as directly exposed to atmosphere and least for evacuated receiver tube.

General trends of results show that efficiency of PTC decreases as wind velocity increases, aperture area increases, ambient temperature decreases, Water inlet temperature increases, mass flow rate decreases, absorber diameter increases. Heat losses increases as wind velocity increases, aperture area increases and ambient. This trend is more predominantly observed for broken tubes as compared to other two cases.

6.1 Simulation Results of Numerical Model

Simulation results of computational model were verified and validated by comparing trends of simulated results with the results found in available literature [28, 32, 38, 39 and 40]. Experimental test results of SEGA LS-2 can be applied to any temperature range b/w T_{amb} and 400 °C having solar irradiance intensity from 100 (W/m^2) to 1100 (W/m^2) and with incident angle modifier range from 0 degree to 60 degrees.[28]

Detailed output results of simulation model by varying one of the operating variables at a time are shown graphically with complete reasoning details below

6.1.1 Trend of output results with variation in Inlet Temperature (T_1)

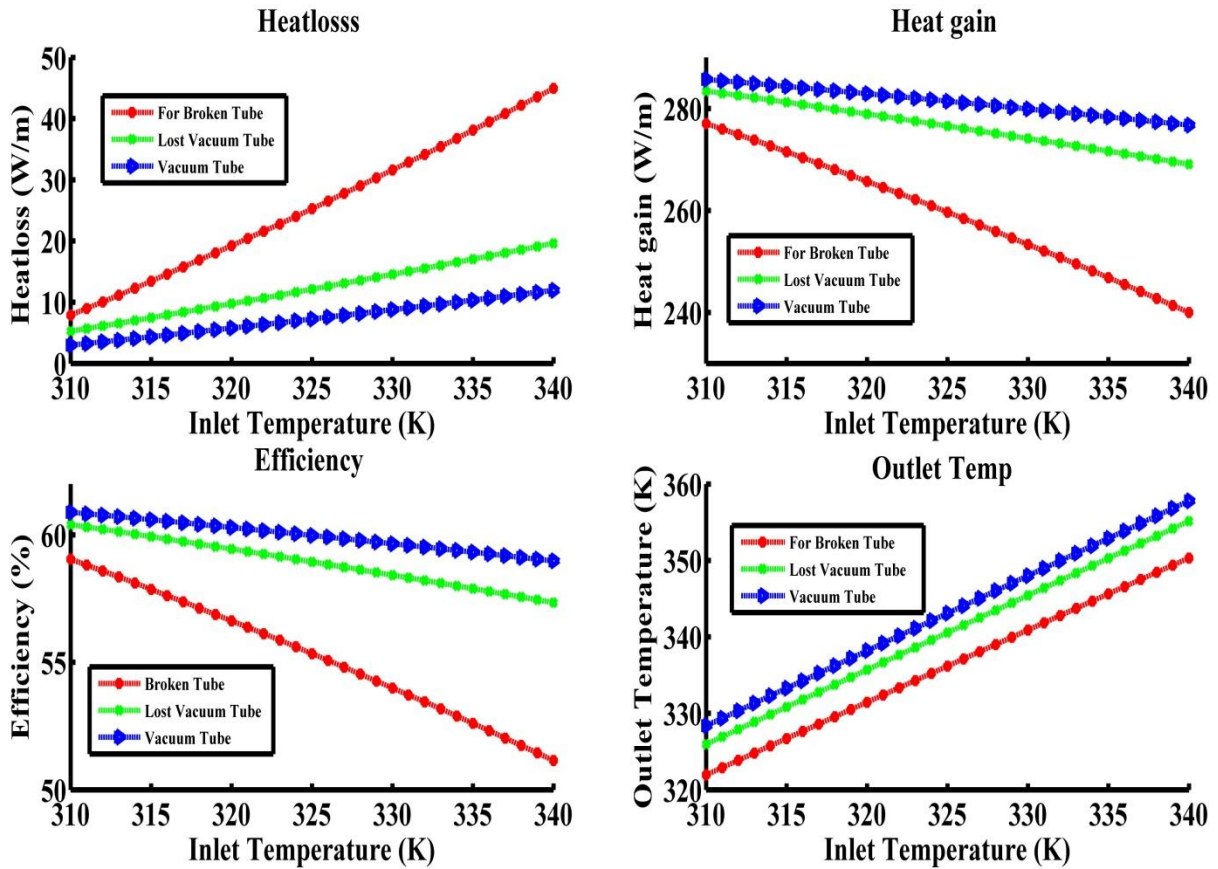


Fig.30. Affect fluid inlet temperature on the performance of PTC

Comparative graphical trend of four performance parameters of PTC as a function of Inlet water temperature (T_1) are shown in **Fig.30**. For all three configurations of absorber tubes heat losses to atmosphere increases as inlet temperature of working fluid increases. This is because higher enthalpy of fluid inside a system means greater heat losses to surrounding due to higher temperature difference. Higher inlet temperature of fluid causes greater heat energy transferred between absorber and envelope surfaces and hence

ultimately higher thermal losses. Higher heat losses cause lower heat gain and reduced efficiency of PTC system. Also higher inlet fluid temperature results in increased outlet fluid temperature with a little heat gain. This affect of inlet fluid temperature is dominated for broken receiver tube as compared to first two cases. The results show that performance of PTC system is adversely affected if absorber tube is broken or lost vacuum as compared to perfect vacuum case. For inlet fluid temperature of 340 K of PTC, evacuated absorber tube case has the dropped efficiency of 58.98 %, lost vacuum case has 57.34 % and broken glass receiver has the lowest efficiency of 51.15 %. Fig 31 depicts trend of percentage efficiency decrease and maximum efficiency achieved as function of inlet temperature. Percentage decrease in efficiency is least for perfect evacuated tube while highest decrease in efficiency is observed for broken absorber glass tube.

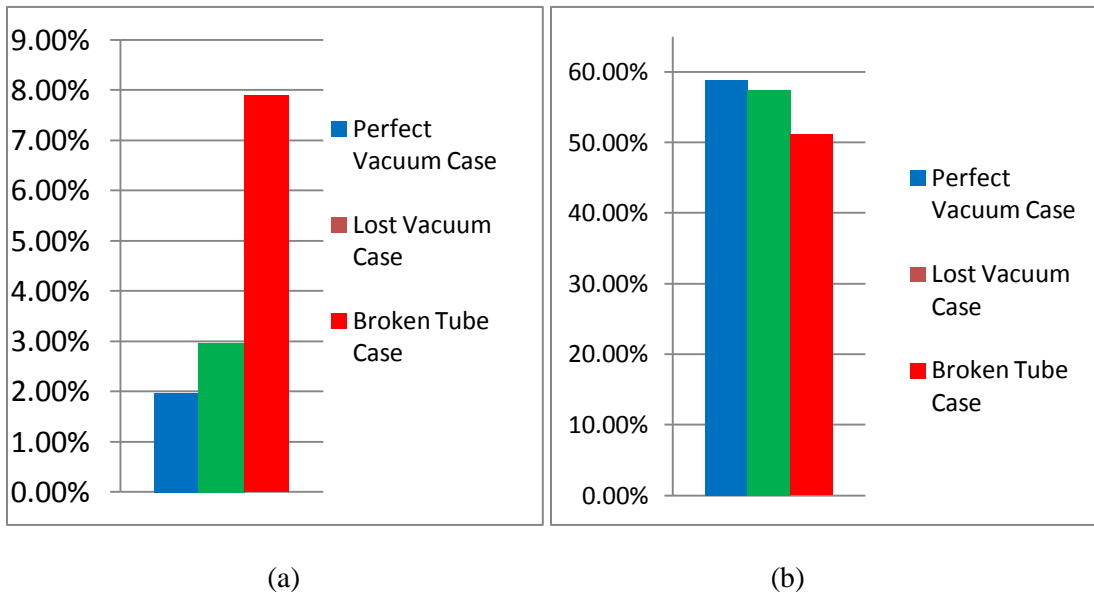


Fig.31 (a) Comparative Percentage drop in efficiency. Fig.31 (b) comparative Maximum efficiency achieved as function of inlet temperature

6.1.2 Trend of output results with variation of Mass flow Rate (\dot{M})

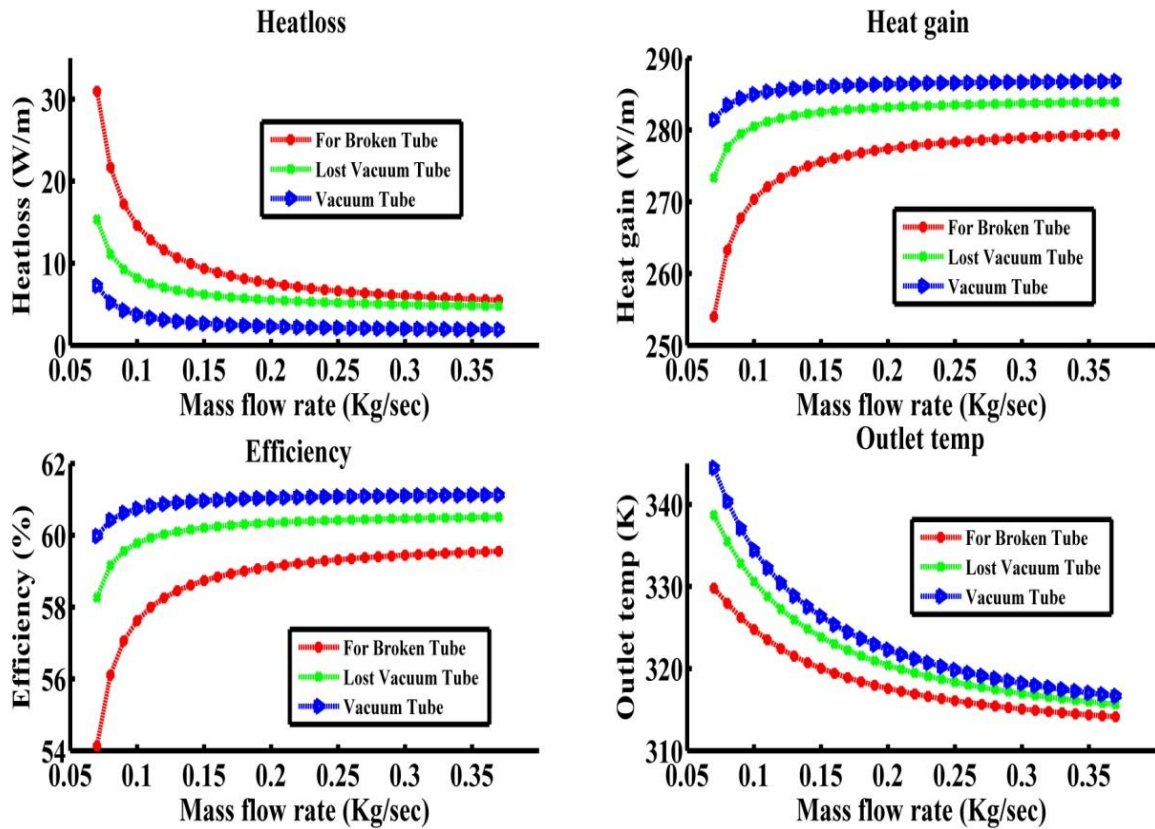


Fig.32. Affect of Mass flow rate on the performance of PTC

For optimized performance of PTC system, It must have optimum flow rate. **Fig.31** shows as mass flow rate (\dot{M}) is increased from .07 (Kg/sec) to 0.37 (Kg/sec), heat losses decreases, heat gain and efficiency increases but outlet temperature of water decreases for the subject three cases. This because higher the mass flow rate means more turbulence in fluid and greater chances of heat energy exchange. But this trend is only limited up to an optimum flow rate after that it becomes. As the graphical data depicts efficiency of PTC increases up to 0.25 (kg/sec) and after that it becomes almost constant. Comparative performance trend reveals that efficiency of PTC is superior using evacuated absorber tube as compared to the other two receiver tube configurations. With mass flow rate of 0.37 (Kg/sec) efficiency of PTC for the considered three cases becomes 61.11%, 60.50%

and 59.55% respectively. Fig 33 depicts trend of percentage efficiency increase and maximum efficiency achieved as function of mass flow rate. Increase in efficiency after optimal flow rate is no more affecting after optimal mass flow rate for all three cases. Highest increase in efficiency is observed for broken absorber tube whereas least increase is for perfect absorber tube. But over all maximum efficiency achieved is for perfect evacuated absorber case.

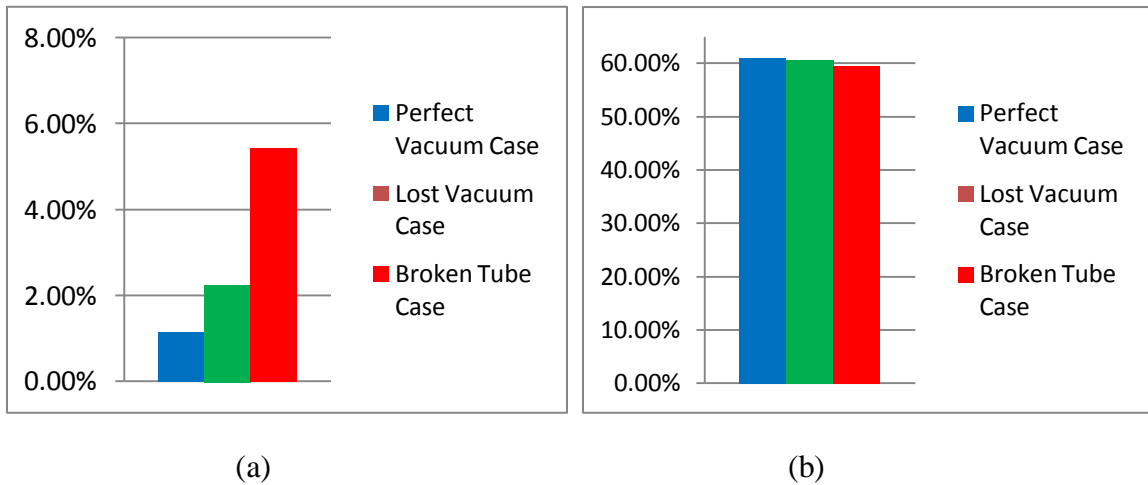


Fig.33 (a) Comparative Percentage drop in efficiency. Fig.33 (b) comparative Maximum efficiency achieved as function of mass flow rate

6.1.3 Trend of output results with variation of Absorber Diameter (D1)

For a fixed aperture area absorber tube needs to have optimal diameter to minimize thermal losses. Performance of PTC decreases for the subject three cases as diameter is increased for fixed aperture width and length but as expected the trend is more dominant for bare absorber pipe. As shown in fig.34 inner diameter (D1) is varied from .024 m to .035 m. Annulus gap diameter (D3-D2) and thickness of absorber circumference (D2-D1) is increased constantly as absorber inner diameter (D1) is increased. Thermal losses increase and heat gain decreases as absorber inner diameter increases due to decreased ratio.

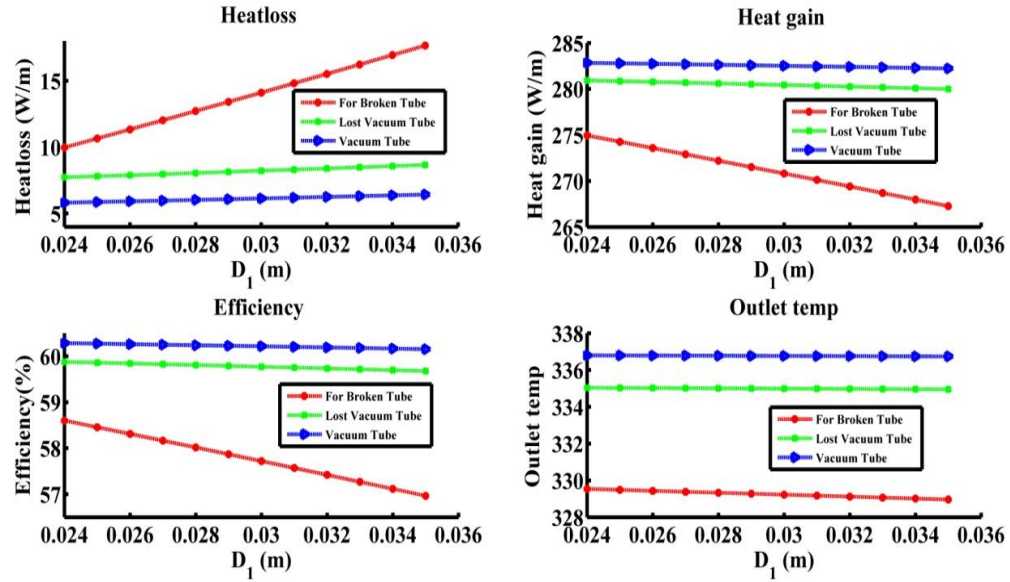


Fig.34. Affect of Absorber diameter on the performance of PTC

Another reason of decreased efficiency of PTC with increased absorber diameter is that greater surface area is available for heat exchange to atmosphere which promotes thermal losses. Heat losses to atmosphere are more dominant for broken absorber tube with abrupt fall in efficiency of PTC as compared to first two discussed cases. The efficiency of PTC is reduced to 60.15 %, 59.67% and 56.96% respectively for considered cases for absorber diameter D_1 of 0.035 m. Fig 35 depicts trend of percentage efficiency increase and maximum efficiency achieved as function absorber tube diameter.

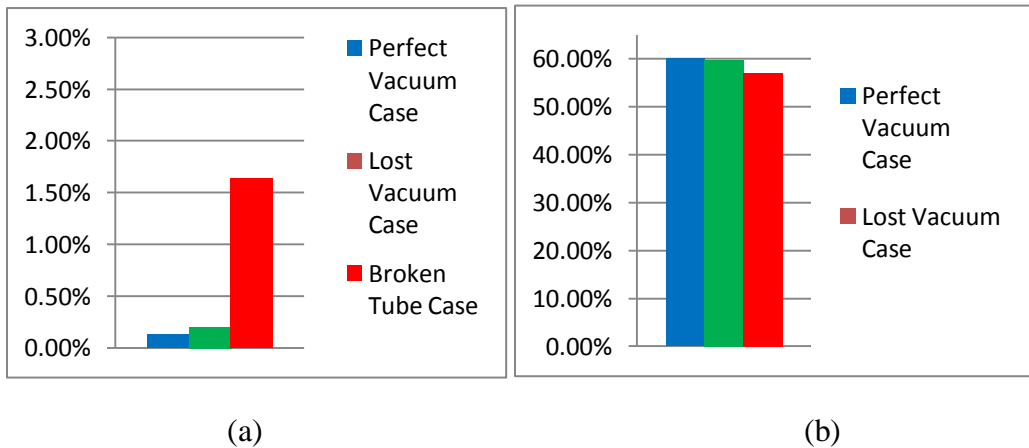


Fig.35 (a) Comparative Percentage drop in efficiency. Fig.35 (b) comparative Maximum efficiency achieved as function of absorber diameter

6.1.4 Trend of output results with variation of Wind speed (Wv)

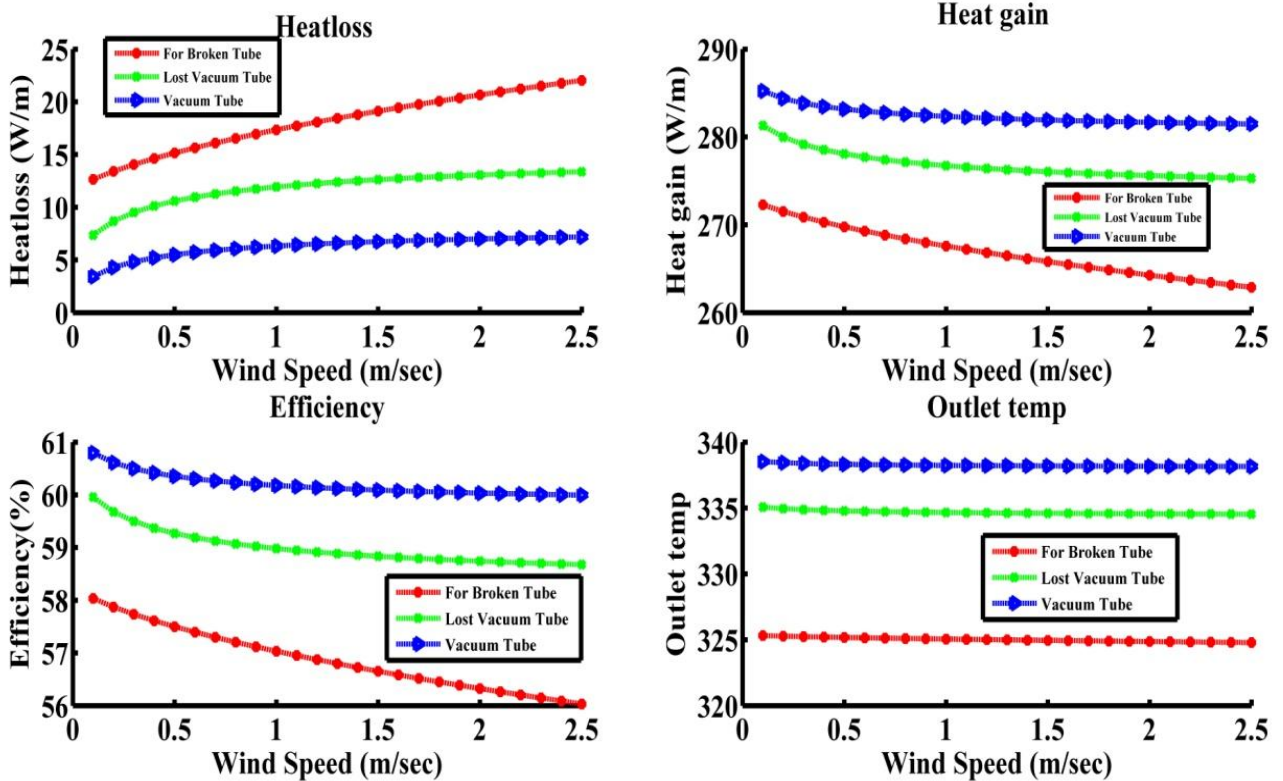


Fig.36. Affect of wind speed on the comparative performance of PTC

Fig.36 depicts the relative performance of PTC for three different configurations of receiver tube as air blowing speed varies from 0.1 (m/sec) to 2.5 (m/sec). The other operating parameters are kept fixed mentioned in Table-5. Wind blowing direction is considered normal to the axis of receiver tube. As the graphical results depict that heat losses increases as wind speed increases for all three configurations. This results in decreased heat gain and fluid (water) outlet temperature. Ultimately efficiency of PTC decreases with increased wind speed. The reason for this trend is that as the wind speed becomes higher, air flow around the circumference of absorber tube becomes more turbulent causing enhanced thermal energy exchange b/w receiver tube surface and ambient air. Thermal losses to atmosphere occur mostly by forced convection and radiation. The simulated results show that for 2.5 (m/sec) wind speed, efficiency of PTC

for perfect vacuum tube is 59.99%, for vacuum breached is 59.94% and for bare absorber with broken envelope is 56.03%. The graphical data show that efficiency of PTC for first two configurations decreases slightly while for bare receiver with broken glass envelope decreases significantly with increased wind speed. This is because in the absence of glass envelope, heat energy transfer takes place directly b/w absorber surface and atmosphere. . Fig 37 depicts trend of percentage efficiency increase and maximum efficiency achieved as function of wind speed.

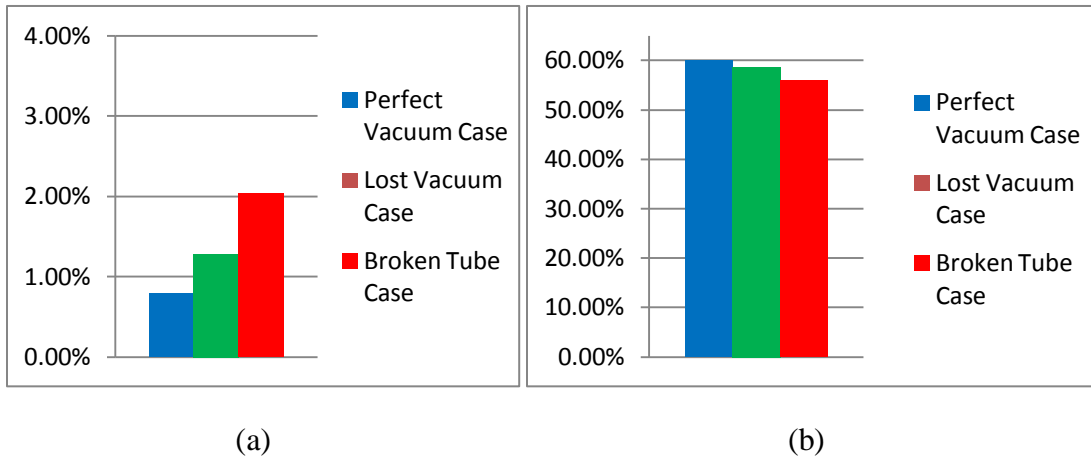


Fig.37 (a) Comparative Percentage drop in efficiency. Fig.37 (b) comparative Maximum efficiency achieved as function of wind speed

6.1.6 Trend of output results with variation of Aperture Area (A_{apert})

Fig.38 shows the affect of aperture area (A_{apert}) on heat loss, heat gain, outlet temperature and efficiency of PTC. For all three configurations of absorber tube heat gain, heat loss and outlet temperature increases as aperture areas increases. This is because as aperture area of PTC increases more surface region is available for solar irradiation collection causing increased concentration ratio. On the contrary thermal losses increase as a function of A_{apert} for considered 3 cases because greater surface area is exposed to atmosphere for radiation and convection heat exchange. For first two discussed cases of absorber tube, ratio of heat gain and incident solar energy decreases very minute and heat losses increase steadily with increasing aperture area.

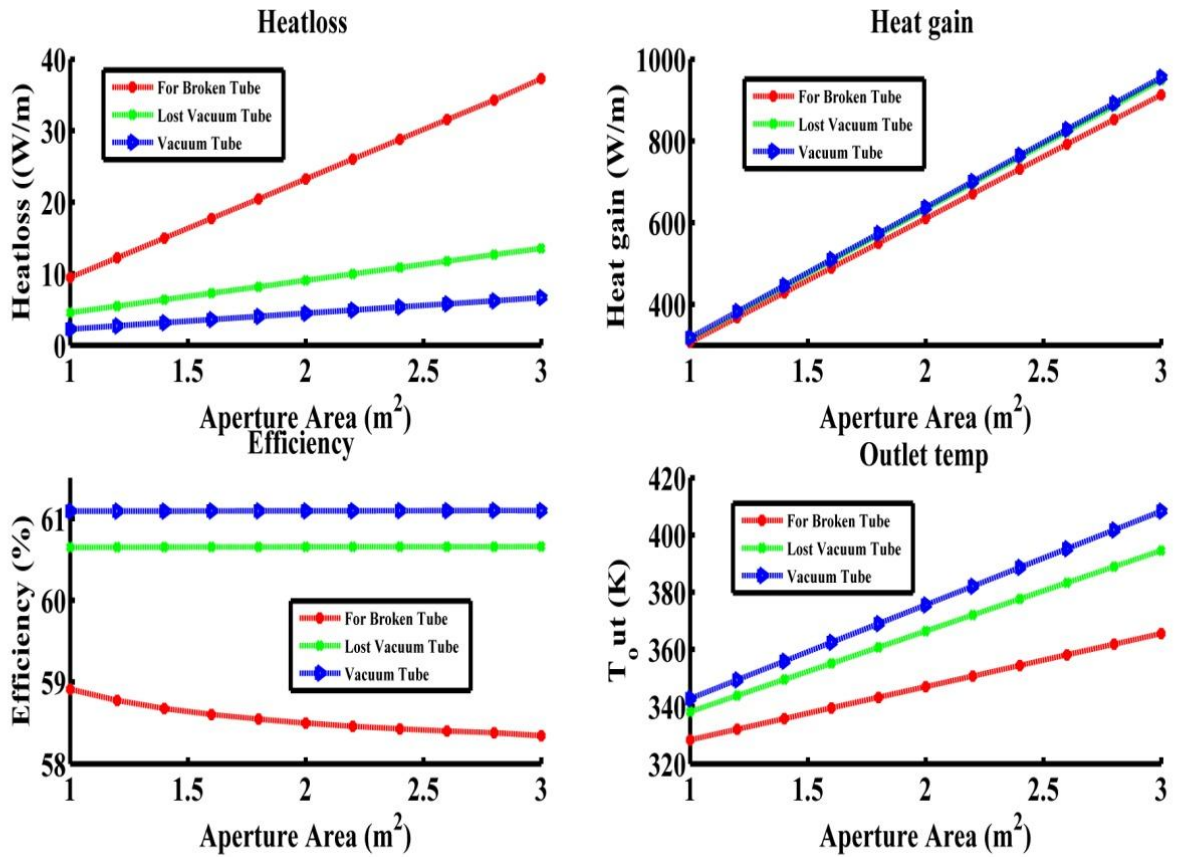


Fig.38. Affect of Aperture area on the performance of PTC

Whereas for broken absorber case study, thermal losses to ambient air are significant resulting in reduced heat gain, outlet temperature and efficiency as compared to first two cases. Simulation results of computational model show that reduced efficiency of three cases is 61.09 %, 60.65 %, 58.34 % respectively with an aperture area of 3 m². Relative performance trend of PTC depict that efficiency of perfect vacuum and lost vacuum absorber case decreases insignificantly, whereas for bare receiver performance of PTC is reduced to unacceptable levels. Fig 39 depicts trend of percentage efficiency increase and maximum efficiency achieved as function of aperture area. Rate of decrease in efficiency as function of aperture is almost negligible but for broken absorber tube it comparatively significant especially when we are dealing with large scale solar thermal power plants.

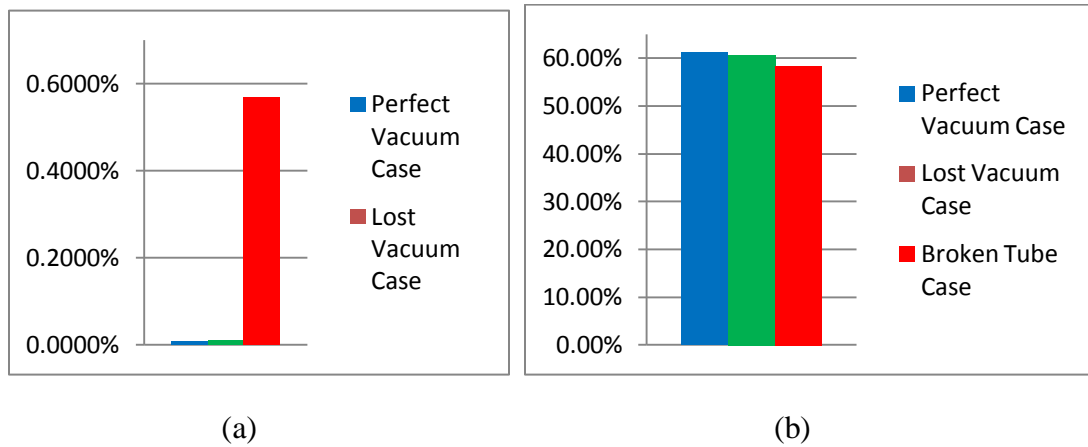


Fig.39 (a) Comparative Percentage drop in efficiency. Fig.39 (b) comparative Maximum efficiency achieved as function of aperture area

6.2 Comparative experimental & simulated Results

Experiments were performed to validate simulation results of the computational model for two parameters that is inlet temperature (T_1) and mass flow rate (\dot{M}). Computational model uses the same boundary conditions as used in experimental setup.

6.2.1 Comparative trend of output results with variation in Inlet Temperature (T_1)

Comparative performance analysis of experimental and simulated results for PTC is illustrated in **Fig.40** as inlet temperature of fluid is varied from 310 K to 340 K. Experimental output data verifies results of numerical model as both results are in close coherence. As the graphical data depicts efficiency and heat gain of PTC decreases, while heat losses and outlet temperature increases as a function of inlet fluid temperature for both experimental and simulation results. The reason for this expected trend has been explained earlier. There is very minute difference between experimental and simulated results but it is very much in acceptable range. Numerically calculated efficiency of PTC for inlet temperature of 340 K for the subject three cases is 58.98 %, 57.34 % and 51.15 % respectively. Whereas when it calculated based on experimental data it comes to be 59.28%, 57.75% and 51.73% respectively and it is very close to simulation result.

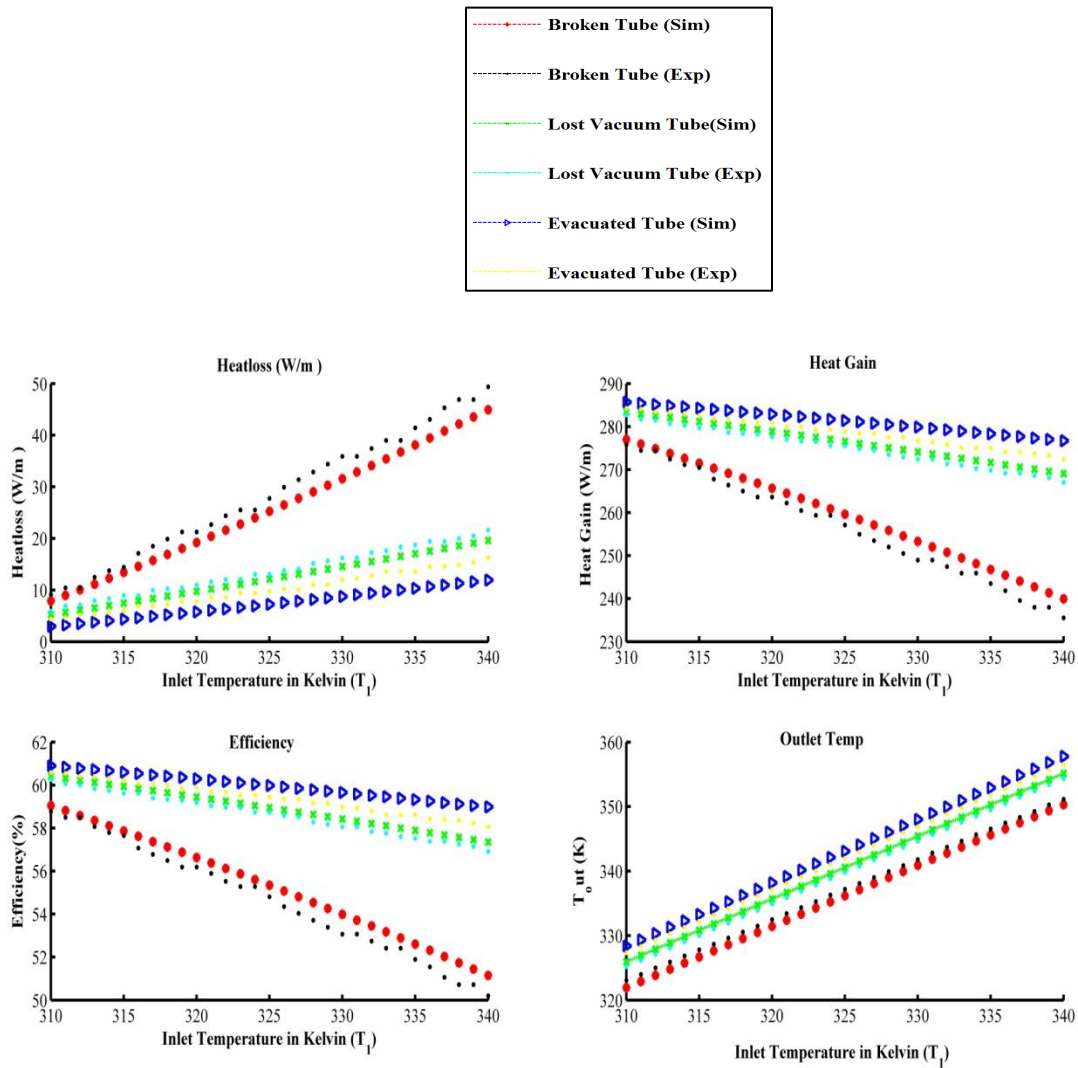


Fig.40 comparative experimental and simulated performance of PTC as function of T_1

6.2.2 Comparative trend of output results with variation in mass flow Rate (\dot{M})

As explained earlier in simulated results efficiency and heat gain of PTC increases while heat losses decreases as function of mass flow rate. Experimental results for the subject three case of PTC also reveal same trend as that of the simulation results and are in close coherence as illustrated in **Fig.41**. There is no affect of mass flow rate on the performance of PTC after optimum mass flow rat that is 0.24 kg/sec. There is minor fluctuation in measured results within acceptable range and it due to measurement

limitations of tools while experimenting. The calculated efficiency of computational model with a flow rate of 0.37% (Kg/sec) for the subject three configurations cases is 61.11%, 60.50% and 59.55% respectively. While experimentally measured results for PTC show the efficiency of 60.95%, 60.64% and 59.61% respectively. Over all comparative performance of numerical model and experimentally measured is shown in **Fig. 41**.

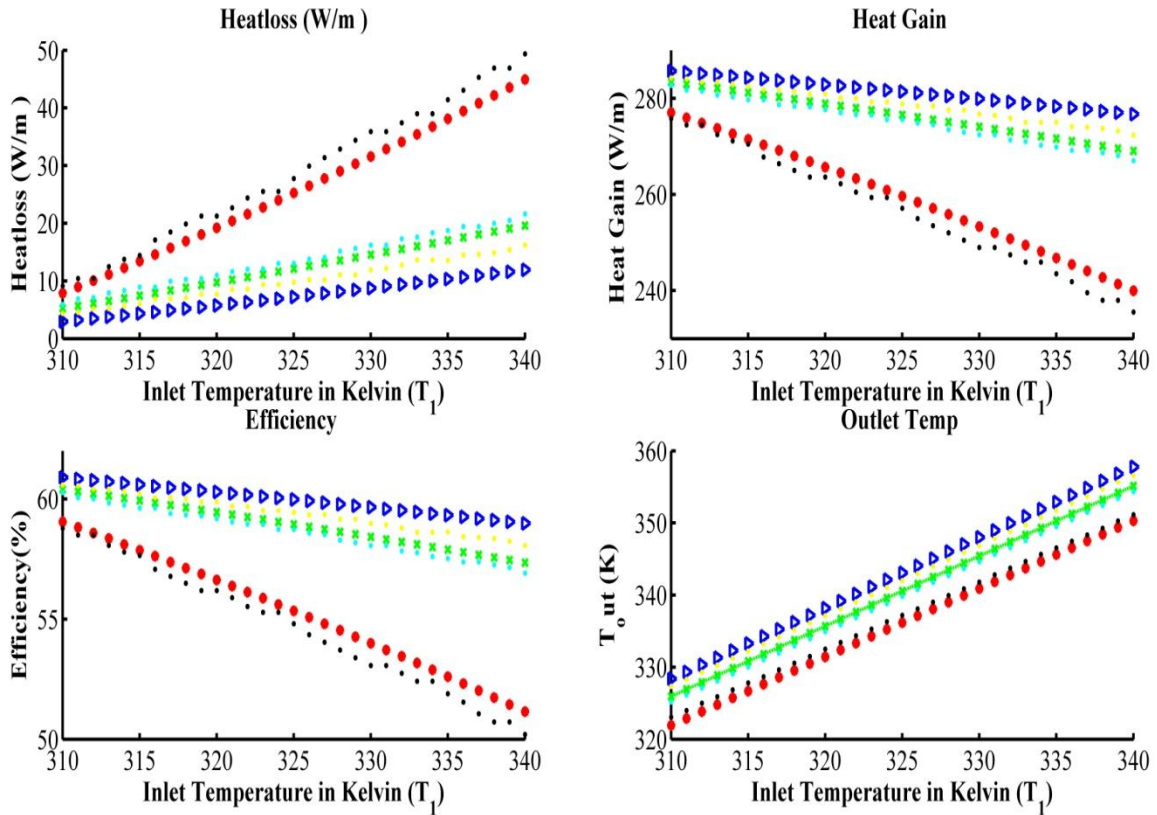


Fig.41 comparative experimental and simulated performance of PTC as function of \dot{M}

CONCLUSION AND RECOMMENDATIONS

7.1 Conclusion

Numerical model and experimental results are used for comparative performance analysis of PTC using three different configurations of absorber tube under meteorological conditions of Islamabad. The subject study gives an idea to designers when is the best time to replace receiver tube of PTC for maximum efficiency. The analysis of results clearly explains the affect of different parameters on heat loss, heat gain, outlet temperature and efficiency of PTC. Experimentation proved that successful concentration of solar irradiation on receiver to grab maximum sun energy greatly depends on geometry design and precision of fabrication process. Study reveals that performance of PTC is adversely affected if receiver tube breaks or it losses vacuum. Maximum thermal energy is transferred to HTF when receiver is working under perfect vacuum as compared to two other receiver configurations. Maximum efficiency drop for three cases is shown in Table 6. Heat losses of PTC are superior for broken receiver case. Thermal losses are mostly by convection and to some extent by radiation. Hence the results show that PTC efficiency is a function discussed five operational parameters.

$$Efficiency_{PTC} = f(T_1, \dot{M}, W_v, D_1, A_{apert})$$

Table-6 Efficiency Drop and Achieved Efficiency of PTC

Parameter	Efficiency Drop	Maximum Efficiency
Inlet temperature	1.98% < 2.95% < 7.9%	58.9% > 57.35% > 51.15%
Mass flow rate	1.14% < 2.25% < 5.43%	61.11% > 60.5% > 59.55%
Wind speed	0.8% < 1.28% < 2.03%	60% > 58.67% > 56%
Ambient temperature	1.99% < 3.11% < 5.18%	61.45 % > 61.03% > 59%
Receiver tube diameter	0.13% < 0.2% < 1.64%	60.15 % > 59.67% > 56.96%
Aperture area	0.0075% < 0.01% < 0.57%	61.09 % > 60.65% > 58.34%

7.2 Recommendations

This thesis study is the first of its kind at School of Mechanical & Manufacturing Engineering (SMME), NUST. The subject thesis focused on study of grabbing maximum solar thermal energy using concentrated solar power (CSP) technology. It finds its applications in commercial and industrial sector where huge thermal energy is utilized and is ideal solution to current power crisis in Pakistan. This thesis topic has opened new avenues at SMME to look into energy sector for future research. Few proposed future research topics related to my thesis are enlisted below

- Study analysis of selective coatings for absorber tubes to reduce emissivity and enhance absorptivity.
- Research scope can be extended to material study of reflecting parabola sheet to enhance optical efficiency of PTC.
- Effective auto tracking of multiple PTC stacks
- Devising CSP technology based energy system for replacing boiler in leather and textile industry.
- Use of Hybrid PTC system for space heating and as a dryer for leather tanning industries.

REFERENCES

- [1] C.-D. Yue, C.-M. Liu, and E. M. L. Liou, "A transition toward a sustainable energy future: feasibility assessment and development strategies of wind power in Taiwan," *Energy Policy*, vol. 29, no. 12, pp. 951–963, Oct. 2001.
- [2] International Energy Agency, "World Energy Outlook 2009," 2009.
- [3] International Energy Agency France (IEA), "Key world energy statistics", 2012. (<http://www.iea.org/publications/freepublications/publication/kwes.pdf>, (accessed in May 2014))
- [4] International Energy Agency, "Key World Energy Statistics," 2010
- [5] Population Clock at Population Census Organization, GoP <http://www.census.gov.pk/index.php> (accessed in Nov 2014)
- [6] A. Malik "Power Crisis in Pakistan: A Crisis in Governance?," *Pakistan Institute of Development Economics*, No. 2012: 4, 2012
- [7] Alternate Energy Development Board, MoWP GoP, Pakistan. <http://www.aedb.org/parl.htm> (accessed in Nov, 2014)
- [8] Hydrocarbon Development Institute of Pakistan (HDIP), "Energy year book 2010," 2011.
- [9] M.A Sheikh, "Renewable energy resource potential in Pakistan," *Renewable and Sustainable Energy Reviews*, vol.9, pp.2696-2702, 2009.
- [10] http://solargis.info/doc/_pics/freemaps/1000px/ghi/SolarGIS-Solar-map-South-And-South-East-Asia-en.png
- [11] Energy Expert Group, Economic advisory council, ministry of finance Pakistan, "Integrated energy plan 2009-2022," Mar 2009.
- [12] S. M. L. Lt, "Sustainable Development " A Critical Review," vol. 19, no. 6, pp. 607–621, 1991.
- [13] I. Purohit and P. Purohit, "Techno-economic evaluation of concentrating solar power generation in India," *Energy Policy*, vol. 38, no. 6, pp. 3015–3029, Jun. 2010.

- [14] R.Manuel, B. Reiner, and P. James , “An Update on Solar Central Receiver Systems, Projects, and Technologies,” *J. Sol. Energy Eng*, vol. 124, pp. 98-108 ,doi:10.1115/1.1467921, 2002
- [15] S.a.Kalogirou, “Solar thermal collectors and applications,” vol. 30, no. 3, pp. 231-295, 2004.
- [16] M. Günther, M. Joemann, and S. Csambor, “Advanced CSP Teaching Materials Chapter 5 Parabolic Trough Technology Authors.”
- [17] V. Dudley, G. Kolb, M. Sloan, and D. Kearney, “SEGS LS2 Solar Collector — Test Results,” Report of Sandia National Laboratories, SANDIA 94-1884, USA, 1994.
- [18] S.D. Odeh, G.L. Morrison, and M. Behnia, “Thermal analysis of parabolic trough solar collector for power generation,” In Proceedings of ANZSES 34th Annual Conference, Darwin, Australia, pp. 460–467, 1996
- [19] D. Yogi Goswami and Feng Xu, “Analysis of a new thermodynamic cycle for combined power and cooling using low and mid temperature solar collectors,” *J. Sol. Energy Eng*, vol. 121, no.2, pp.91–98, 1999.
- [20] C. E. Kennedy, “Review of Mid- to High- Temperature Solar Selective Absorber Materials Review of Mid- to High- Temperature Solar Selective Absorber Materials,” Technical Report: NREL/TP-520- 3126. July, 2002.
- [21] F. Burkholder and C. Kutscher, “Heat Loss Testing of Schott ’ s 2008 PTR70 Parabolic Trough,” NREL/ TP-550-45633, May, 2009.
- [22] L. S. W. Muhlen, B. Najafi, F. Rinaldi, and R. Marchesi, “Sensitivity analysis on the effect of key parameters on the performance of parabolic trough solar collectors,” *J. Phys. Conf. Ser.*, vol. 501, p. 012032, Apr. 2014.
- [23] L. Valenzuela, R. López-Martín, and E. Zarza, “Optical and thermal performance of large-size parabolic-trough solar collectors from outdoor experiments: A test method and a case study,” *Energy*, vol. 70, pp. 456–464, Jun. 2014.

- [24] P. Venkataramaiah, P. Mohana Reddy, and P. Sairam, "Simulation and optimisation studies on a solar parabolic collector: an experimental investigation," *Int. J. Sustain. Energy*, no. January 2014, pp. 1–14, Jun. 2013.
- [25] R. V. Padilla, A. Fontalvo, G. Demirkaya, A. Martinez, and A. G. Quiroga, "Exergy analysis of parabolic trough solar receiver," *Appl. Therm. Eng.*, vol. 67, no. 1–2, pp. 579–586, Jun. 2014.
- [26] M. Günther, M. Joemann, and S. Csambor, "Advanced CSP Teaching Materials Chapter 5 Parabolic Trough Technology."
- [27] D. Lipp, "Parabolic Trough Solar Collector Analysis Developing the Trough Characterization," vol. 124, no. February, pp. 1–11, 2008
- [28] R. Forristall, "Heat Transfer Analysis and Modeling of a Parabolic Trough Solar Receiver Implemented in Engineering Equation Solver," NREL/ TP-550-34169, October, 2003
- [29] <https://eosweb.larc.nasa.gov/cgi-bin/sse/sse.cgi?skip@larc.nasa.gov+s01#s01> (Accessed on 15 Oct 2014)
- [30] J. A. Duffie & W. A. Beckman, "*Solar Engineering Of Thermal Processes*," John Wiley & Sons. INC.
- [31] H. Price, "Concentrated Solar Power Use in Africa," NREL/TP. Golden, CO: National Renewable Energy Laboratory, 2001
- [32] Y. S.Touloukian, D. P.DeWitt, "Radiative Properties, Nonmetallic Solids. Thermophysical Properties of Matter", Vol. 8, New York. Plenum Publishing, 1972
- [33] V. Gnielinski, "New Equations for Heat and Mass Transfer in Turbulent Pipe and Channel Flow," *International Chemical Engineering*, vol.16, no.2, pp. 359–363, April 1976.
- [34] F.P.Incropera, D.P.DeWitt, "Fundamentals of Heat and Mass Transfer," Third Edition, NY: John Wiley and Sons, New York, 1990.
- [35] KJC Operating Company "Final Report on HCE Heat Transfer Analysis Code," SANDIA Contract No. AB-0227. Albuquerque, NM: Sandia National Laboratories, December 1993.

- [36] A.C. Ratzel, C.E.Hickox, and D.K.Gartling, "Techniques for Reducing Thermal Conduction and Natural Convection Heat Losses in Annular Receiver Geometries," *Journal of Heat Transfer*, vol.101, no.1, pp. 108–113, February 1979.
- [37] A. Bejan, "Convection Heat Transfer", Second Edition, NY: John Wiley & Sons, New York, 1995.
- [38] P. Daniel, Y. Joshi, and A. K. Das, "Numerical investigation of parabolic trough receiver performance with outer vacuum shell," *Sol. Energy*, vol. 85, no. 9, pp. 1910–1914, Sep. 2011
- [39] M. Hernández-Román, A. Manzano-Ramírez, J. Pineda-Piñón, and J. Ortega-Moody, "Exergetic and Thermo-economic Analyses of Solar Air Heating Processes Using a Parabolic Trough Collector," *Entropy*, vol. 16, no. 8, pp. 4612–4625, Aug. 2014.
- [40] M. Yaghoubi, F. Ahmadi, and M. Bandehee, "Analysis of Heat Losses of Absorber Tubes of Parabolic through Collector of Shiraz (Iran) Solar Power Plant," *J. Clean Energy Technol.*, vol. 1, no. 1, pp. 33–37, 2013.

**APPENDIX I: METEOROLOGICAL DATA OF EXPERIMENTATION
SITE**